

Inside the black box: Neural network-based real-time prediction of US recessions

Seulki Chung^a

^a*GSEFM, Department of Empirical Economics, Technische Universität
Darmstadt, Karolinenpl.5, Darmstadt, 64289, Germany*

Abstract

A standard feedforward neural network (FFN) and two specific types of recurrent neural networks, long short-term memory (LSTM) and gated recurrent unit (GRU), are used for modeling US recessions in the period from 1967 to 2021. The estimated models are then employed to conduct real-time predictions of the Great Recession and the Covid-19 recession in the US. Their predictive performances are compared to those of the traditional linear models, the standard logit model and the ridge logit model. The out-of-sample performance suggests the application of LSTM and GRU in the area of recession forecasting, especially for the long-term forecasting tasks. They outperform other types of models across five different forecast horizons with respect to a selected set of statistical metrics. Shapley additive explanations (SHAP) method is applied to GRU and the ridge logit model as the best performer in the neural network and linear model group, respectively, to gain insight into the variable importance. The evaluation of variable importance differs between GRU and the ridge logit model, as reflected in their unequal variable orders determined by the SHAP values. These different weight assignments can be attributed to GRU's flexibility and capability to capture the business cycle asymmetries and nonlinearities. The SHAP method delivers some key recession indicators. For forecasting up to 3 months, the stock price index, real GDP, and private residential fixed investment show great short-term predictability, while for longer-term forecasting up to 12 months, the term spread and the producer price index have strong explanatory power for recessions. These findings are robust against other interpretation methods such as the local interpretable model-agnostic explanations (LIME) for GRU and the marginal effects for the ridge logit model.

Keywords: Forecasting, Recession, Business cycle, LSTM, GRU, SHAP, LIME

JEL: C01, C45, C51, C52, C53, C71, E37

October 27, 2023

1. Introduction

Recession forecasting has been a longstanding challenge for policymakers and market practitioners, as it enables them to make timely decisions that could mitigate the impact of a recession. However, due to the intricate and interconnected nature of modern economics, this task has proven to be difficult and has had limited success. Traditional linear methods such as probit or logit models, along with their variations and extensions, have been widely employed for this forecasting task. However, in recent decades, machine learning techniques, including artificial neural networks, have become increasingly popular among economists and have been applied to certain macroeconomic forecasting problems. Nevertheless, it has yet to be demonstrated whether and why these modern approaches allow for informed deviation from conventional linear models, when it comes to predicting recessions.

Since the pioneering work of [Mitchell and Burns \(1938\)](#), which identified 21 variables out of a larger set as potential economic indicators for business cycles out of a larger set, researchers have been engaged in selecting indicators and developing theoretical frameworks or predictive models to link these indicators with business cycles. However, most studies have primarily focused on linear frameworks. Many of them have utilized probit regression models or their extensions to generate recession forecasts. [Estrella and Mishkin \(1996, 1998\)](#) compiled a combination of financial and macroeconomic variables and conducted recession forecasting using a probit framework. Their findings revealed that stock prices exhibit greater short-term predictability, while the slope of the yield curve performs better for longer-term predictions. [Wright \(2006\)](#) demonstrated that probit models incorporating the federal funds rate and term spread as predictors outperform models solely relying on the term spread. [Dueker \(1997, 2002\)](#) expanded the standard probit model by incorporating Markov regime switching within the probit framework, allowing for variation in coefficients. [Chauvet and Potter \(2005\)](#) introduced several specifications to the probit model that accounted for different business cycle dependencies and autocorrelation errors, concluding that their more complicated extensions improved the accuracy of recession forecasts. [Fornari and Lemke \(2010\)](#) as well as [Nyberg \(2014\)](#) incorporated vector autoregression components into the probit model to capture the endogenous dynamics of the predictors.

While probit regression and its extensions continue to be widely used in business cycle forecasting, there has been a growing interest in exploring the forecasting capabilities of nonlinear models,

including machine learning methods. This interest stems from the recognition that the business cycle often exhibits asymmetric and nonlinear patterns (Acemoglu and Scott (1997); Morley and Piger (2012)). Empirical evidence supports this notion, such as the work of Tiao and Tsay (1994), who demonstrate that a threshold autoregressive model outperforms a linear autoregressive model for predicting GDP growth. Maasoumi et al. (1994) examine multiple macroeconomic time series and confirm their nonlinear nature. Puglia and Tucker (2021) highlight the attractiveness of machine learning methods as an alternative to probit regression and its extensions, noting that probit methods typically require additional parameters for flexibility, whereas flexibility is inherent in machine learning methods. Stock and Watson (1998) compare the forecasting performance of 49 univariate linear and nonlinear models across 215 macroeconomic time series. They find that some of the nonlinear models perform poorly compared to linear models. Jaditz et al. (1998) explore the use of nearest neighbor regression models for forecasting industrial production but observe only marginal improvements in predictive performance. Vishwanathan and Murty (2002) present an iterative algorithm for support vector machines in classification problems. Ng (2014) applies a tree ensemble classifier to a large panel of predictors. Fornaro (2016) combines a Bayesian methodology with a shrinkage prior within the probit framework to predict recessions using extensive sets of predictors. More recently, Holopainen and Sarlin (2017), Bluwstein et al. (2020), and Vrontos et al. (2021) employ various machine learning methods for economic event forecasting. Vrontos et al. (2021) provide empirical evidence supporting the application of machine learning over traditional econometric techniques in the context of recession forecasting.

Neural networks, as a subfield of machine learning, have garnered significant attention and application in fields like finance, primarily due to their ability to establish flexible mappings between variables and exhibit high pattern recognition capabilities (Zhang et al. (1998)). Neural networks, being highly nonlinear and nonparametric models, can approximate almost any functional form accurately, as stated by the universal approximation theorem (Hornik et al. (1989)), given that the network is wide or deep enough. Consequently, they are valuable modeling tools, particularly when there is limited prior knowledge about the appropriate functional relationships. However, the utilization of neural networks in macroeconomic studies has been relatively limited due to the small sample sizes and low-frequency nature of macroeconomic data. Swanson and White (1997) compare artificial neural networks with linear models in terms of predictive performance for nine

macroeconomic variables, revealing only marginal improvements in forecast accuracy. [Moshiri and Cameron \(2000\)](#) apply neural networks to inflation forecasting using a dataset of 300 observations spanning 25 years of monthly data. [Tkacz \(2001\)](#) compares multivariate neural networks with linear and univariate models, finding minor forecast improvements in the short term but more pronounced benefits for longer horizons, such as a one-year forecast. [Qi \(2001\)](#) employs a simple feed-forward neural network to predict US recessions using a range of financial and economic indicators, identifying some indicators as useful for prediction. More recently, [Puglia and Tucker \(2021\)](#) compare neural networks with probit regression in forecasting US recessions using the term spread and other macro-financial variables, finding little difference between the models when evaluated. [Wang et al. \(2022\)](#) employ a specific type of recurrent neural network, namely a Bi-LSTM with autoencoder, along with other machine learning models to predict the beginning and end of economic recessions in the US. Their results suggest that the Bi-LSTM with autoencoder is the most accurate model.

The novelty of this paper is twofold: Firstly, it focuses on two special types of recurrent neural networks, the long short-term memory (LSTM) and the gated recurrent unit (GRU), which address the limitations of a standard recurrent neural network related to the exploding and vanishing gradient problems. Their performance is compared to the simple feedforward neural network (FFN) that suffer from the key limitation of having to specify the temporal dependence upfront in the design of the model and to the traditional linear models in the context of recession forecasting. Secondly, the paper applies the Shapley additive explanations method (SHAP) to GRU which shows higher overall performance than LSTM, to explore the variable importance for different forecast horizons. In the context of recession forecasting, [Puglia and Tucker \(2021\)](#) and [Delgado et al. \(2022\)](#) also use the SHAP method to decompose recession forecasts, but they are applied to other models than LSTM and GRU. The three main findings can be summarized as follows: Firstly, the out-of-sample performance strongly supports the application of LSTM and GRU in the area of recession forecasting, especially for the long-term forecasting tasks. They outperform other types of models across five forecast horizons with respect to different types of statistical performance metrics. Secondly, GRU and the ridge logit model differ in assessing variable importance, evident in the different variable orders based on the SHAP values. Lastly, while the leading predictors for GRU and ridge logit models slightly differ, key indicators like S&P 500 index, real GDP,

and private residential fixed investment consistently emerge for short-term predictions (up to 3 months). For longer-term forecasts (6 months or more), the term spread and producer price index take precedence. These results are corroborated by local interpretable model-agnostic explanations (LIME) and marginal effects, respectively.

The remainder of the paper is as follows. Section 2 explains the data used. Section 3 describes the models and performance evaluation metrics and outlines the research methodology. Section 4 presents the prediction results. Section 5 reports the methodology and results of SHAP and other interpretation methods, and Section 6 concludes.

2. Data

Prior studies in business cycle forecasting often rely on macroeconomic indicators, which are subject to revisions after their initial estimates. [Stark and Croushore \(2002\)](#) demonstrate that the accuracy of forecasts is influenced by using the most up-to-date data instead of real-time data. Therefore, when comparing forecasts from new models to benchmark forecasts, it is crucial to ensure that the comparisons are based on real-time data. In my research, the focus is primarily on assessing the real-time predictability of neural network models with respect to the Great Recession and the Covid-19 recession in the United States. This necessitates working with real-time data since the information that is available in hindsight was not accessible prior to the recessions. To evaluate the predictability of the recessions, I utilize the same data that actually was available to real-time forecasters for out-of-sample forecasting.

The dataset employed for prediction consists of 194 real-time vintages of macroeconomic and financial market variables, covering the period from February 1967 to October 2021. The out-of-sample forecasting commences in November 2006, utilizing the real-time vintage of data. Taking into account previous studies like [Vrontos et al. \(2021\)](#) and the availability of real-time data, a set of 25 predictors is chosen. A detailed list with descriptions of these variables can be found in Table 1.

The selected predictors cover a wide range of categories, including output, income, prices, the labor market, the housing market, money and credit, and the financial market. The data frequency varies from daily to quarterly. To facilitate model estimation, higher frequency data is aggregated into monthly data using the mean. Quarterly frequency variables are transformed into monthly

Table 1: Overview of predictors

Nr.	Predictive variable	Abbreviation	Category	Transformation	Frequency
1	Average hourly earnings of production and nonsupervisory employees	AHETPI	Income	Percent change	Monthly
2	Average weekly hours of production and nonsupervisory employees	AWHNONAG	Labor market	percent change	Monthly
3	Moody's BAA yield	BAA	Money and credit	First-order difference	Monthly
4	Moody's BAA yield relative to 10-Year treasury yield	BAA10YM	Money and credit	First-order difference	Monthly
5	Real manufacturing and trade industries sales	CMRMTSPL	Output	Log growth rate	Monthly
6	Corporate profits after tax	CP	Income	Log growth rate	Quarterly
7	Real disposable personal income	DSPIC96	Income	Log growth rate	Monthly
8	Effective federal funds rate	FEDFUNDS	Financial market	First-order difference	Monthly
9	Real gross domestic product	GDPC1	Output	Log growth rate	Quarterly
10	Privately-owned housing units started	HOUST	Housing market	Log growth rate	Monthly
11	Industrial production index	INDPRO	Output	Log growth rate	Monthly
12	Real M1 money stock	M1REAL	Money and credit	First-order difference	Monthly
13	Real M2 money stock	M2REAL	Money and credit	First-order difference	Monthly
14	Non-farm payroll total	PAYEMS	Labor market	Log growth rate	Monthly
15	Real personal consumption expenditures	PCEC96	Prices	Log growth rate	Monthly
16	Privately-owned housing units permitted	PERMIT	Housing market	Log growth rate	Monthly
17	Producer price index by all commodities	PPIACO	Prices	Log growth rate	Monthly
18	Private residential fixed investment	PRFI	Housing market	Log growth rate	Quarterly
19	S&P 500 index	SP500	Financial market	Log growth rate	Daily
20	3-month treasury bill rate	TB3MS	Financial market	First-order difference	Monthly
21	Term spread - 5-year treasury yield minus 3-month treasury bill rate	T5Y3MM	Financial market	First-order difference	Monthly
22	Consumer Sentiment - University of Michigan	UMCSENT	Prices	Log growth rate	Monthly
23	Unemployment rate	UNRATE	Labor market	First-order difference	Monthly
24	Producer price index by commodity: final demand: finished goods	WPSFD49207	Prices	Log growth rate	Monthly
25	Real personal income excluding current transfer receipts	W875RX1	Income	Log growth rate	Monthly

The table presents a list of predictive variables in alphabetical order based on their abbreviations according to ALFRED. It includes information about their respective categories, transformations applied to ensure stationarity, and their original data frequency.

equivalents using natural cubic spline interpolation. Specifically, at each month, all available data up to that point are used to calculate the interpolating cubic spline. This spline curve is then utilized to generate data of monthly frequency that lie on the curve between the quarterly data points.

The majority of monthly data vintages for the variables are obtained from Archival Federal Reserve Economic Data (ALFRED). However, there are a few selected predictors for which the real-time data prior to 2013 is not available in ALFRED. The first set of variables, including real personal income excluding transfer receipts and real manufacturing and trade sales, along with total non-farm payroll employment and the industrial production index, are used by [Chauvet and](#)

Piger (2008) to identify business cycle dates in real time. The real-time data for these series, provided by Jeremy Piger on his website, ends in August 2013. However, it can be easily extended beyond 2013 by using the data in ALFRED. The second set of variables consists of real M1 and M2 money stock, for which the earliest available real-time data in ALFRED is from January 2014. To address the absence of real-time vintages for real M1 and M2 money stock before this date, nominal M1 and M2 money stock are adjusted for inflation using the consumer price index, which has real-time vintages readily accessible in ALFRED.

To identify recession periods in the United States, I rely on the business cycle expansion and contraction dates determined by the National Bureau of Economic Research (NBER). NBER is widely regarded as the standard reference for US business cycles in the existing literature. In this study, recession months are defined as the period following the peak and continuing until the trough, while all other months are considered periods of economic expansion. The earliest available vintage of NBER recession indicator in ALFRED is from September 2014. For the monthly vintages preceding that date, I manually collect and construct them based on the official announcements made by the NBER business cycle dating committee¹. However, it's worth noting that one major practical challenge with NBER business cycle dates is that they are often announced with significant publication delays.

Table 2 presents the peak and trough dates of the US business cycle from 1980 to 2021, along with their corresponding announcement dates. The publication lags for the recessions listed in the table range from 5 to 21 months, with troughs being identified later than peaks on average. While the NBER business cycle dates remain unchanged once finalized, the presence of publication lags complicates the creation of real-time versions of the NBER recession indicator. To address this, the NBER recession indicator in ALFRED is constructed under the assumption that the previous state remains unchanged until a new turning point is officially announced.

3. Econometric methodology

In this section, the focus is on the technical aspects of the models used to predict the two most recent recessions in the United States. The paper specifically explores neural networks, which are complex nonlinear models composed of interconnected nodes arranged in multiple layers. These

¹<https://www.nber.org/research/business-cycle-dating/business-cycle-dating-committee-announcements>

Table 2: US Business Cycle dates

Date	Type	Duration	Announcement
1980:01	Peak	6	1980:06(+5)
1980:07	Trough	12	1981:07(+12)
1981:07	Peak	16	1982:01(+6)
1982:11	Trough	92	1983:07(+8)
1990:07	Peak	8	1991:04(+9)
1991:03	Trough	120	1992:12(+21)
2001:03	Peak	8	2001:11(+8)
2001:11	Trough	73	2003:07(+20)
2007:12	Peak	18	2008:12(+12)
2009:06	Trough	128	2010:09(+15)
2020:02	Peak	2	2020:06(+4)
2020:04	Trough	ongoing	2021:07(+15)

The table reports NBER business cycle dates, including the type of cycle (contraction or expansion), the duration in months, and the time of announcement. The data covers the period from 1980 to 2021, and publication lags in months are indicated in parentheses.

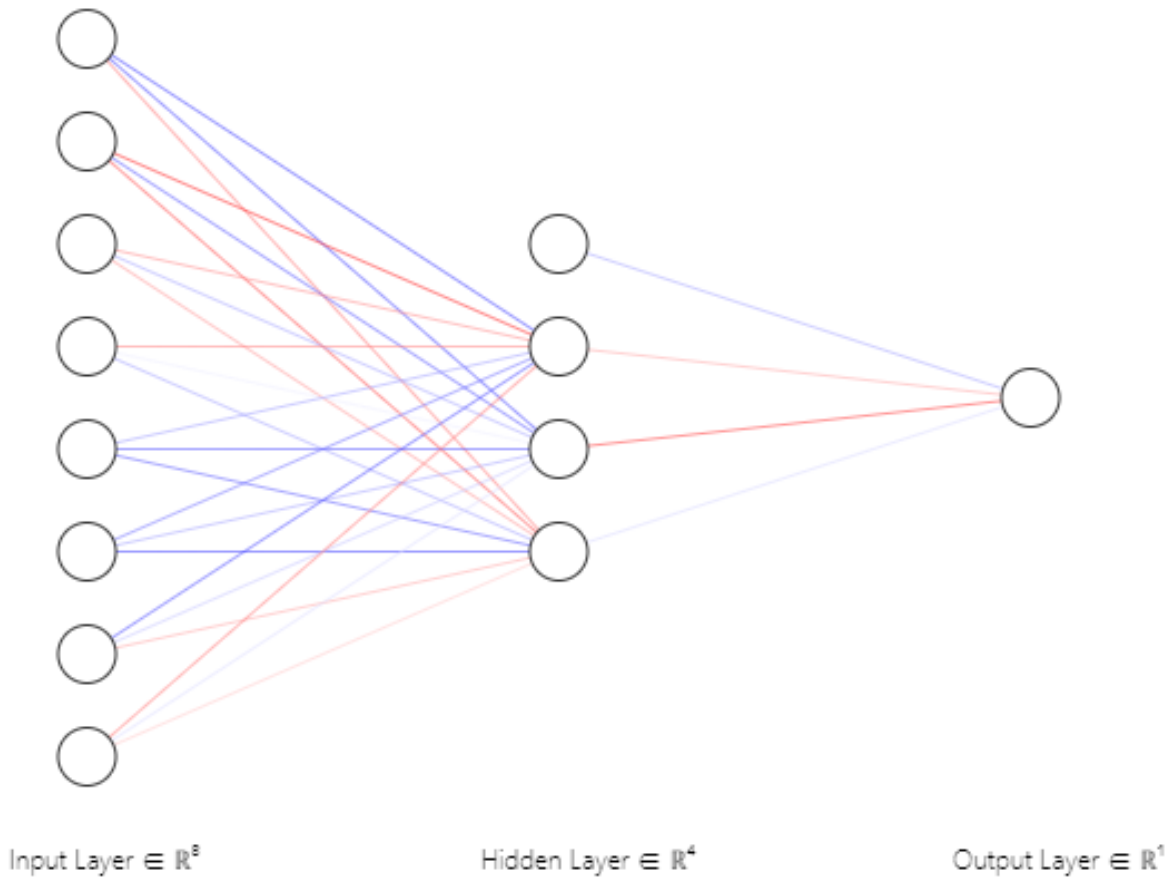
networks have the ability to approximate any linear or nonlinear continuous functions, as stated by the universal approximation theorem ([Hornik et al. \(1989\)](#)), given that the network is wide or deep enough. In this paper, three types of neural networks are employed for recession forecasting: feedforward neural network (FFN), long short-term memory (LSTM), and gated recurrent unit (GRU). Section 3.1 provides a detailed description of these models. Model specifications, including estimation and prediction techniques, are discussed in Section 3.2. Finally, Section 3.3 introduces statistical measures that effectively evaluate the prediction performance.

3.1. Neural Networks

3.1.1. Feedforward neural network

FFN is a widely used and straightforward type of artificial neural network. It consists of multiple processing units called nodes or neurons that are organized into layers. It operates by transmitting information in a unidirectional manner, where data flows from the input layer to the

Figure 1: The architecture of a feed-forward neural network



The figure illustrates an example of a feed-forward neural network featuring one hidden layer and bias units. The output layer consists of a single unit that uses a sigmoid function for activation, catering to a binary classification task. For the sake of illustration, the edges are depicted in different colors to indicate diverse edge weights, which can be either positive or negative, and also in different opacities to highlight varying magnitudes of the edge weights.

output layer without feedback loops. Figure 1 illustrates, based on the NN-SVG ², an example of a three-layer FFN designed for binary classification. It comprises an input layer with eight units, a hidden layer with four units, and an output layer with one unit. The first units in the input and hidden layers serve as bias units. In this configuration, data from the input layer is passed through the hidden layer, which transforms the data. The values obtained from the hidden layer are then

²Lenail (2019) <https://doi.org/10.21105/joss.00747>

forwarded to the output layer, which translates them into desired outputs based on the problem at hand. In the case of binary classification, the last unit in the output layer utilizes a sigmoid activation function, producing a value between 0 and 1. This value represents the probability of an event occurring.

Depending on the number of explanatory variables in the data and the number of units in the hidden layer the unknown underlying function f for an output node can be written as

$$f(X) = g_2 \left[\alpha_0 + \sum_{j=1}^k \alpha_j g_1 \left(\beta_{0j} + \sum_{i=1}^n \beta_{ij} x_i \right) \right] + \epsilon,$$

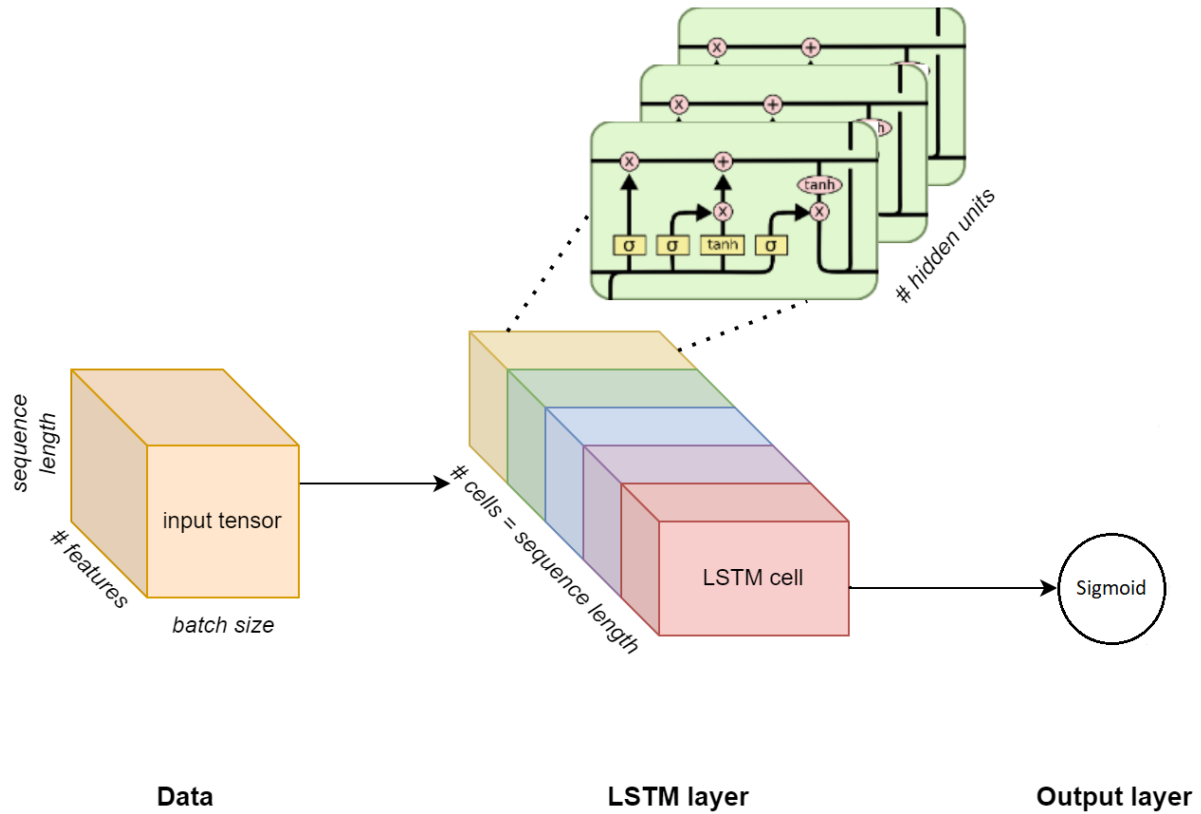
where n is the number of predictors, k is the number of units in the hidden layer, g_1 is the activation function in the hidden layer, g_2 is the activation function in the output layer, β_{ij} and α_j represent the weight parameters from the input to the hidden layer and from the hidden to the output layer, respectively, and ϵ is the error term. The weight parameters are estimated by the backpropagation process that seeks to repeatedly update the weights until convergence based on the derivatives of the cost function with respect to input and the hidden layers.

3.1.2. Long short-term memory

FFN is restricted to one-way signal flow, meaning that there is no feedback mechanism where the output of a layer can influence the same layer. Consequently, FFN lacks the ability to capture temporal dependencies in time series data. Although time series data can be fed into a FFN by incorporating additional input units representing previous time points, the main limitation lies in the fixed dimensionality of inputs and outputs. In other words, the precise length of temporal dependence must be predetermined, which is often unknown in real-world scenarios. This is where RNN comes into play. RNN establishes connections that form cycles, allowing for feedback loops where data can be fed back into the input before being forwarded again. This feedback loop enables RNN to maintain an internal state or memory to process sequences of inputs or time steps. Theoretically, RNN can retain all information over time and handle long-term dependencies. However, they face two computational challenges. Firstly, as input sequences grow longer, the backpropagation process relies heavily on the chain rule, which may lead to vanishing gradients. If any gradient approaches zero, all other gradients will diminish exponentially fast due to the multiplicative nature of the chain rule. This phenomenon, known as the vanishing gradient problem, prevents effective training in the model. Secondly, depending on the length of input sequences,

the gradient of the loss function can become excessively large and result in numerical instability, referred to as the exploding gradient problem.

Figure 2: The architecture of a long short-term memory network

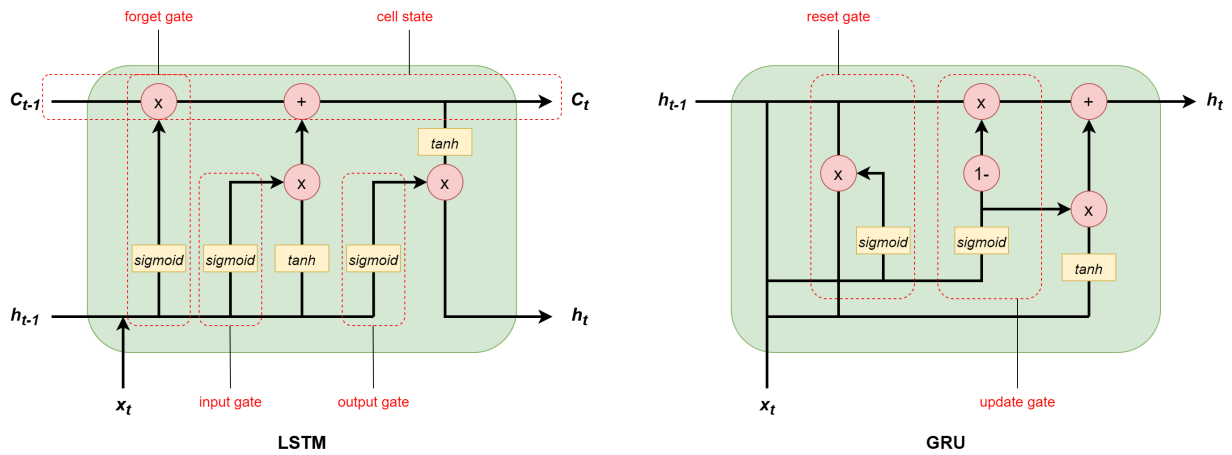


The figure depicts a basic LSTM neural network architecture, comprising a LSTM layer and an output layer. The data is represented as a three-dimensional tensor, with dimensions for batch size, variables, and time steps. Each LSTM cell in the LSTM layer handles information retrieval at a specific time point using specialized processing gates in the hidden units.

[Hochreiter and Schmidhuber \(1997\)](#) introduced the long short-term memory (LSTM) architecture and a corresponding learning algorithm to address the challenges of error back-flow and long-term dependency in RNN. Figure 2 illustrates a basic LSTM neural network comprising a LSTM layer and an output layer. The input data is represented by a three-dimensional tensor, with dimensions for batch size, variables, and time steps. The LSTM layer consists of as many LSTM cells as there are time steps, with each cell responsible for information retrieval at a specific

time point in a time series. These cells contain hidden units comprising special nodes and gates that are designed to process the information. Figure 3 provides a closer look at the hidden units of LSTM and GRU. For both Figure 2 and 3, the graphics of the hidden units are adapted from Chris Colah’s blog³. The LSTM unit on the left variables three gates (forget, input, and output gates) denoted by red dotted lines, along with a cell state, which is a crucial distinction between RNN and LSTM network. The cell state functions like a conveyor belt that extends across the entire sequence, facilitating the retention of information over long periods. This mechanism closely resembles the long-term memory function of the human brain. The three gates regulate the flow of information to and from the cell state, enhancing the overall functionality of the network.

Figure 3: Hidden units of a LSTM and a GRU network with specialized gates



The figure displays the hidden units of LSTM and GRU network in comparison to each other. The LSTM unit has three gates (forget, input, and output) and a cell state, distinguishing it from RNN. The cell state acts as a conveyor belt for retaining information over time, similar to human long-term memory, while the gates control information flow for improved network functionality. The GRU simplifies the LSTM structure by merging two gates into a single gate and combining the cell and hidden state. It replaces the output gate with an update gate that processes new information in relation to the previous hidden state and updates it accordingly.

Upon the encounter of information from the previous time step h_{t-1} with new information x_t , the forget gate evaluates which information from the cell state C_{t-1} should be discarded. Formally, this can be described as follows:

³<https://colah.github.io/posts/2015-08-Understanding-LSTMs/>

$$f_t = \sigma(W_f \cdot [h_{t-1} \ x_t] + b_f).$$

This equation presents a concise representation of the mathematical operations within the forget gate. The terms enclosed in brackets represent the linear operations within the activation function, introducing nonlinearity. The input vector $[h_{t-1} \ x_t]$ is multiplied by the weight matrix W_f and combined with the bias vector b_f , which are then passed through the activation function, typically a sigmoid function. This ensures that the output values fall within the range from 0 to 1. Later, these values will be multiplied by each corresponding element in the previous cell state C_{t-1} , determining the proportion of old information to be retained in the new cell state.

The subsequent step involves identifying the portion of new information deemed valuable for storage in the cell state. This process occurs in two stages. Firstly, a node utilizing the hyperbolic tangent function proposes a vector of new candidate values for the cell state, denoted as \tilde{C}_t :

$$\tilde{C}_t = \tanh(W_C \cdot [h_{t-1} \ x_t] + b_C).$$

Secondly, the input gate regulates the magnitude of the update, determining which values of \tilde{C}_t will be stored in the cell state C_t :

$$i_t = \sigma(W_i \cdot [h_{t-1} \ x_t] + b_i).$$

Similarly, the input gate generates values ranging from 0 to 1, which, when multiplied by \tilde{C}_t , determine the proportion of the new candidate that should be incorporated into the cell state:

$$C_t = f_t \times C_{t-1} + i_t \times \tilde{C}_t.$$

This equation provides a summary of the update process. The new cell state C_t is obtained by combining the previous state C_{t-1} multiplied by the forget gate f_t , which discards irrelevant information from the old state, and the new candidate values \tilde{C}_t scaled by the input gate i_t , retaining only the most important information from the new candidate state.

The new hidden state h_t is determined by the current cell state C_t and the output gate o_t :

$$o_t = \sigma(W_o \cdot [h_{t-1} \ x_t] + b_o).$$

The output gate in this equation utilizes a sigmoid activation function to determine the portion of the new cell state that will be outputted:

$$h_t = o_t \times \tanh(C_t).$$

The cell state undergoes the hyperbolic tangent function and is subsequently multiplied by the output of the output gate, yielding the new hidden state h_t . Therefore, h_t selectively captures the most pertinent information from the cell state, representing the short-term memory, while the cell state retains the long-term memory.

3.1.3. Gated recurrent unit

In Figure 3, the right panel depicts a gated recurrent unit (GRU) which differs from the LSTM in terms of the structure and quantity of its gates. GRU, introduced by [Cho et al. \(2014\)](#), aims to simplify the LSTM by combining two gates into a single gate and merging the cell state with the hidden state. Unlike LSTM, GRU eliminates the output gate and integrates the functions of the forget and input gates into a single gate known as the update gate. This update gate processes new information based on the previous hidden state, consequently updating the hidden state.

Initially, the previous hidden state h_{t-1} and the current input x_t are introduced and passed through the reset gate, which determines the extent to which past information should be disregarded:

$$r_t = \sigma(W_r \cdot [h_{t-1} \ x_t] + b_r).$$

As the sigmoid activation function outputs values between 0 and 1, the resulting values can be interpreted as the proportion of past information to retain. This value, denoted as r_t , is multiplied by h_{t-1} and passed through the hyperbolic tangent (\tanh) activation function. This process yields a vector of new candidate values, represented as \tilde{h}_t :

$$\tilde{h}_t = \tanh(W_h \cdot [r_t \cdot h_{t-1} \ x_t] + b_h).$$

The update gate governs the decision of which information to update in the next step:

$$z_t = \sigma(W_z \cdot [h_{t-1} \ x_t] + b_z).$$

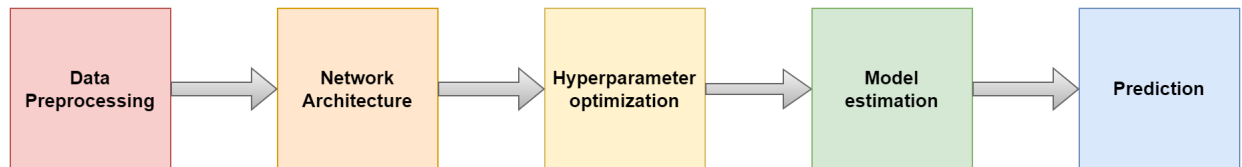
Finally, the new hidden state h_t is then computed as a weighted average of the previous hidden state h_{t-1} and the new candidate values \tilde{h}_t :

$$h_t = (1 - z_t) \cdot h_{t-1} + z_t \cdot \tilde{h}_t.$$

3.2. Model specifications

Before estimating the model, it is necessary to prepare the chosen type of neural network. Figure 4 illustrates a simplified workflow chart outlining the process of forecasting using neural networks. Recession forecasting using neural networks involves five steps: Data must first undergo preprocessing before being fed into the model. Depending on the specific type of neural networks the network architecture is chosen. Hyperparameters are then optimized using the time series cross-validation in expanding window scheme. The second and third steps can be combined, treating the number of layers and units within those layers as hyperparameters. Once the data is prepared and the optimal set of hyperparameters is determined, the model is ready to be estimated and generate predictions.

Figure 4: Workflow chart of the forecasting process



Data preprocessing

The first step involves preprocessing the data before it can be fed into the model. This preprocessing stage comprises multiple smaller steps. Initially, each series is evaluated and transformed individually to ensure stationarity. [Zhang et al. \(2020\)](#) argue that while advanced neural network-based optimization algorithms can handle non-stationary data, they incorporate historical gradients in the update calculations, which can result in a lack of relevance to past information when dealing with non-stationary data where distributions change over time. Therefore, it is prudent to use stationary time series data. The second step involves seasonally adjusting and standardizing all explanatory variables. Lastly, a generator function is employed to generate data batches throughout the estimation process. Data batches are sets of data that are processed all at once. Optimization algorithms based on stochastic gradient descent often utilize smaller batch sizes or minibatches. [Bottou \(2010\)](#) and [Ge et al. \(2015\)](#) highlight that minibatches offer the advantage of avoiding memory loss and introducing sufficient noise into each gradient update, aiding in escaping saddle points or local minima while achieving faster convergence.

Occasionally, data may have time delays or missing values. In such cases, a k -nearest-neighbor imputation method is used during the data pre-processing stage. Experimenting with alternative methods, such as the bagged tree imputation algorithm, does not affect the results significantly, although the latter is known for its superior performance on account of higher computational costs according to [Stekhoven and Bühlmann \(2011\)](#).

Additionally, the LSTM and GRU networks require a three-dimensional tensor as input, consisting of the batch size, the number of variables, and the number of time steps as axes. To accommodate LSTM and GRU network, the generator function transforms the data into a suitable three-dimensional tensor format. To fully utilize the capacity of neural networks, all 12 monthly lags of the predictors are included. [De Veaux and Ungar \(1994\)](#) argue that due to the overparameterization of neural networks, individual weights associated with multicollinearity become less influential. The final output of a neural network is a result of various combinations of activation functions that involve interactions among predictors, making the impact of multicollinearity typically insignificant. Moreover, the backpropagation algorithm used in neural networks does not require inverting matrices, which can be problematic when there is perfect or severe multicollinearity.

Network architecture

In Section 3.1, three neural network models are presented, each based on a different architecture. The number of units in the input layer is determined by the number of variables. Depending on the desired number of time points to consider, the input dimension increases accordingly. For example, if the last 12 months of data from 25 predictors are to be used for future predictions, the input dimension would increase from 25 to $25 \times 12 = 300$. Given the relatively small dataset with a maximum of 657 observations across 25 explanatory variables, a maximum of two hidden layers for FFN and one hidden layer for LSTM and GRU is allowed. The number of hidden layers and the number of units in those layers are treated as hyperparameters that should be optimized during the cross-validation process, which will be discussed in more detail later. Both the input and hidden layers of FFN use the rectified linear unit as the activation function for their units. The output layer consists of a single unit that uses the sigmoid activation function, producing a number between 0 and 1. This number can be interpreted as the probability of a recession.

As illustrated in Figure 2, the LSTM neural network architecture consists of as many LSTM cells as the number of time steps to look back. In the context of recession forecasting, I choose to examine the temporal variations of the predictors over the last 12 months, which corresponds to 12 lagged variables of the same predictor. Hence, there are 12 LSTM cells, each with a same number of hidden units ranging from 16 to 64. The first unit in the first LSTM cell is linked to the first unit in the second LSTM cell, and the same holds for the rest of the LSTM cells. This approach ensures that each chain of units explores different variable dimensions at different time points. Additionally, the network may require a second chain of cells, leading to a hidden or stacked LSTM layer. The optimal number of stacked layers is determined by the hyperparameter optimization process. The output layer in LSTM is the same as in FFN. GRU follows the same architecture as LSTM but differs in the structure and functionality of the hidden units within the GRU network.

Hyperparameter optimization

Deep neural networks with multiple hidden layers have the capacity to learn complex relationships. However, when training data are limited, some of these relationships may be the outcome of sampling noise and might not be present in real test data. This gives rise to overfitting, which

occurs when a model fails to generalize from observed data to new data. Overfitting is a commonly acknowledged challenge in the supervised machine learning framework, and various methods employing different strategies have been devised to mitigate its effects and prevent the model from overfitting. [Ying \(2019\)](#) categorizes methods to address overfitting into four groups: network reduction, data augmentation, early stopping, and regularization.

Network reduction involves reducing the depth and width of a neural network by decreasing the number of layers and units, thereby reducing the total number of parameters to estimate. This approach helps the model focus on capturing essential patterns in the training data, leading to a better generalization of test data. To implement network reduction, the network is limited to a maximum of one or two hidden layers, depending on the types of models, and a relatively small number of units is chosen for these layers. Additionally, through cross-validation, the model selects the optimal depth and width that minimizes validation loss, ensuring good generalization on unseen validation data.

Complex models with numerous parameters require a substantial amount of data to distinguish meaningful patterns from noise. Therefore, expanding the training data is an effective approach to enhance the model's generalizability. Data augmentation involves not only acquiring more training data but also employing techniques directly applied to the existing data, such as random sampling or reshuffling. I am unable to address this issue due to two reasons. Firstly, I use the same data as in chapter 2 to compare the performance of neural networks with traditional statistical models like logistic regression. Therefore, data augmentation is not suitable as it would distort the actual performance. Secondly, the temporal dependence of the time series data across multiple variables is a crucial aspect that needs to be explored. In this context, data augmentation strategies such as random sampling or reshuffling are not desirable.

Instead, early stopping is implemented as a strategy to halt the training process when the gap between training loss and validation loss begins to widen. The parameters are then set to the values corresponding to the smallest gap, preventing the model from excessively memorizing the training data. This helps in improving the model's performance on unseen data. To incorporate early stopping, a call is included during the estimation process that stops the iteration and restores the best parameters when the validation loss does not decrease for 5 consecutive epochs during cross-validation and for 10 consecutive epochs during the final estimation, where an epoch means

one complete pass of the training dataset through the algorithm.

Regularization is a technique used to mitigate the impact of less important variables in a model. There are two commonly applied categories of regularization methods in neural networks. The first category involves adding a penalty term or regularizer to the loss function. Two well-known types of regularizers, namely $L1$ and $L2$, are commonly used, similar to their application in penalized regression. $L1$ regularization, known as Lasso regression (Tibshirani (1996)), assigns zero weights to unimportant variables, effectively removing them from the model. This ensures that only influential variables with significant effects on the variable of interest are retained. On the other hand, $L2$ regularization, known as Ridge regression (Hoerl and Kennard (1970)), assigns lower weights to unimportant variables rather than discarding them completely. This approach aims to extract as much relevant information as possible while controlling model complexity and reducing overfitting. In my model, I incorporate $L2$ regularization to address these concerns, as chapter 2 demonstrated the superiority of Ridge regression over Lasso regression in the context of recession forecasting. The second category of regularization methods involves using a technique called dropout. Dropout was introduced by Srivastava et al. (2014) and involves randomly dropping units and their connections from the neural network during training. A certain percentage of hidden units are randomly dropped to create a thinned network, which is then trained using stochastic gradient descent. After training, the dropped units are restored, and the process is repeated. Dropout can be seen as approximating the effects of averaging the estimates over multiple smaller networks, while also preventing overfitting. I leverage the dropout technique in my model, treating the dropout percentage as a hyperparameter to be optimized through cross-validation.

Apart from the hyperparameters related to the overfitting issue, neural networks also have other hyperparameters that need to be determined prior to training. These hyperparameters include the number of layers, the number of units in these layers, batch size, and learning rate. The values of these hyperparameters must be specified before training can begin. There are various methods to search for the best combination of hyperparameters, known as hyperparameter optimization. One simple approach is manual search, where the researchers select their own set of hyperparameters based on existing literature and evaluate the model performance on validation data. This process is repeated with different hyperparameter settings until the best combination is found. However, manual search can be time-consuming and does not guarantee finding the optimal hyperparam-

ters. Grid search is another approach, where a predetermined set of values is specified for each hyperparameter. Every possible combination of values is then evaluated, resulting in a large number of trials. However, as indicated by [Bellman \(1961\)](#), the number of possible combinations grows exponentially with the number of hyperparameters, leading to the curse of dimensionality. This can make grid search impractical for models with many hyperparameters. A more effective approach, demonstrated by [Bergstra and Bengio \(2012\)](#), is random search. Random search involves randomly selecting values from predetermined ranges for each hyperparameter. The advantage of random search is that it can identify a good or even better set of hyperparameters within a smaller fraction of computation time compared to manual or grid search methods. Following this approach, the random search is conducted using predefined ranges of values for the hyperparameters. The types of hyperparameters and their specific ranges used for random search in the optimization process are reported in Table 3.

Table 3: Tuning hyperparameters

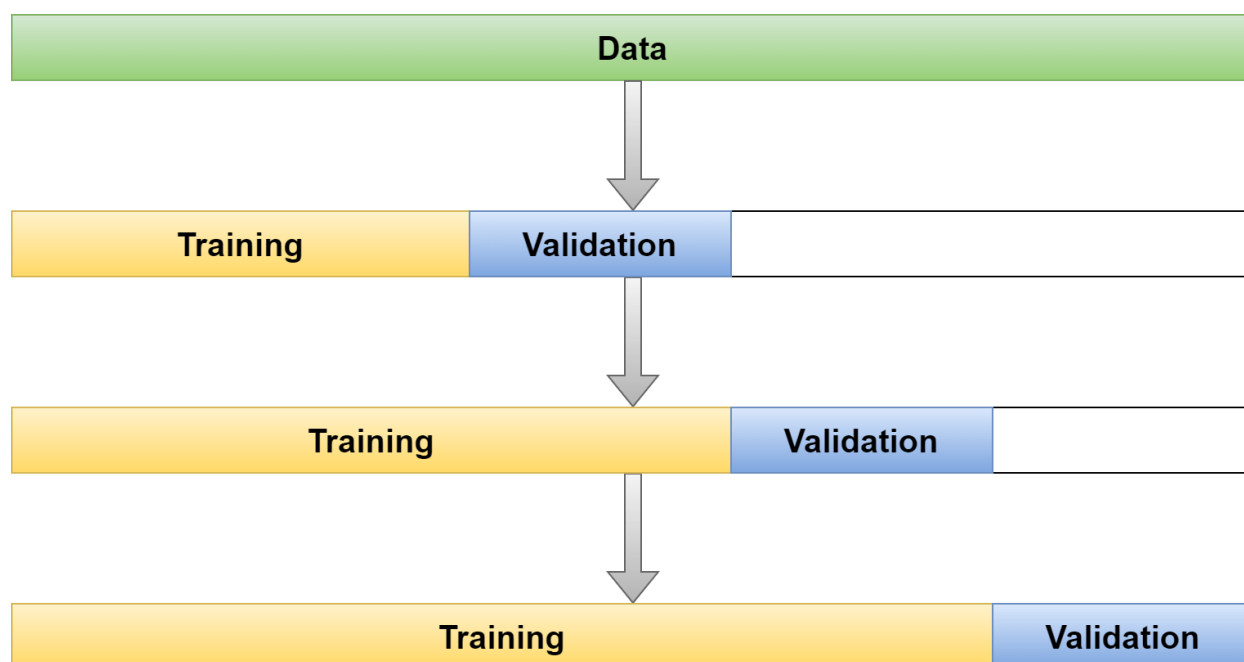
Type	Range
# hidden layer	$\in \{1, 2\}$
# unit	$\in \{16, 32, 64\}$
batch size	$\in \{16, 32, 64\}$
dropout	$\in \{0, 0.1, 0.2, 0.3, 0.4, 0.5\}$
recurrent dropout	$\in \{0, 0.1, 0.2, 0.3, 0.4, 0.5\}$
weight decay	$\in \{0, 0.1, 0.2\}$
learning rate	$\in \{0.01, 0.001\}$

The table provides the ranges of possible values for different neural network-based hyperparameters of the neural networks used in the analysis. The optimal combination of these hyperparameters is obtained by random search using the time series cross-validation technique in expanding window scheme.

Figure 5 illustrates the form of cross-validation that is employed to determine the optimal set of hyperparameters. Each block of the training set is divided into two sections at every iteration, with the validation set always coming after the training split. This approach ensures that the natural order of observations is maintained. For each block, the size of the validation set remains the same, while the training set gets larger as the validation set of the prior block is added to it. The number

of iterations in the cross-validation setup depends on the size of each block. If the block size is small, the number of blocks and iterations increases. However, selecting an excessively small block size may result in certain blocks having insufficient or no recession data, leading to sampling bias. Considering the information presented in Table 2, which indicates the longest period between two recessions in US history prior to the Great Recession as 128 months, the length of each validation block is set to be 128 months to ensure that each validation set contains data from at least one recession. The length l of the first training block is equal to $l = N_{total} - 128 \times (\lfloor \frac{N_{total}}{128} \rfloor - 1)$, where N_{total} denotes the total number of observations in a data vintage. This guarantees that the first training block is always larger than the validation block. Subsequently, an expanding window approach is adopted, increasing the length of the training set by 128 months at each step while maintaining a validation block of the same length (128 months). This methodology ensures that scarce recession data are fully utilized.

Figure 5: Cross-validation for time series



The figure illustrates the form of cross-validation. Each block of the training set is divided into two parts, and the training set is always before the validation set to preserve the natural order of observations within each block. The size of the validation set remains constant for each block, while the training set grows larger as the prior block's validation set is incorporated into it.

For each combination of hyperparameters, the average validation loss across all cross-validations is computed and stored. The set of hyperparameters with the lowest average validation loss is selected as the optimal choice. According to mathematical calculations by [Bergstra and Bengio \(2012\)](#), using random search with 60 trials is likely to yield a set of hyperparameters that falls within the top 5% interval around the optimal solution with a 95% probability. Therefore, 60 trials are conducted for each training process. Once the optimal combination of hyperparameters is determined, the entire dataset is split into training and validation part in the same proportion, maintaining the chronological order of the data. Afterwards, the final estimation and validation of the model is performed to improve the accuracy of the parameters and check for any signs of overfitting.

Model estimation

Once the hyperparameters are optimized, the neural network is prepared to fit the training data. The data is fed into the model, processed, and transformed into an output. This output is then compared to the actual output, and the error signals are propagated backward through the network to adjust the parameters accordingly. This iterative process is known as backpropagation and continues until a specific condition is satisfied. Although the concept appears straightforward, the estimation process involves extensive mathematical computations. The parameter values are estimated to minimize the following binary cross-entropy loss function:

$$\text{Loss} = \frac{1}{n} \sum_{i=1}^N -[y_i \cdot \ln(p_i) + (1 - y_i) \cdot \ln(1 - p_i)].$$

In most cases, there is no analytical solution available for minimizing such problems, and therefore the parameters need to be estimated numerically. To perform this estimation, I utilize the Adam optimizer, which was introduced by [Kingma and Ba \(2014\)](#). The Adam optimizer is specifically designed for optimizing stochastic loss functions using first-order gradients. It combines the strengths of two popular optimization methods, AdaGrad ([Duchi et al. \(2011\)](#)) and RMSProp ([Tieleman and Hinton \(2012\)](#)). The Adam optimizer offers computational efficiency and requires minimal memory resources.

Prediction

Since the effectiveness of predictive variables may vary across different forecast horizons, I explore five distinct windows: nowcasting, immediate-term, short-term, medium-term, and long-term. These windows correspond to predicting the current month, one month ahead, three months ahead, six months ahead, and twelve months ahead, respectively. Accounting for the two-month publication lag, the forecast horizons represent 2-, 3-, 5-, 8-, and 14-steps-ahead forecasts using the real-time set of predictive variables. For example, suppose it is November 2006, and I have data available up to September 2006, which was published in October 2006. If I aim to conduct nowcasting and forecast the recession for the current month, I use all available data up to September 2006 to predict for November 2006, resulting in a two-steps-ahead forecast. Similarly, for other forecast horizons, two extra months or steps need to be considered.

After the models generate probability predictions, they are transformed into monthly zero-one indicators that represent the state of the economy, recession or boom, based on predefined cut-points. The conventional approach is to use a fixed threshold, typically set at 0.5. Under this approach, if a probability prediction is equal to or greater than 0.5, it is classified as a recession, and vice versa. However, it is often mentioned that business cycles exhibit asymmetry, and therefore a 50% threshold may not be optimal for linear modeling methods. [Berge and Jorda \(2011\)](#) propose an optimal cutpoint within the range of 0.3 to 0.6 based on smoothed state probabilities estimated by [Chauvet and Piger \(2008\)](#). [Ng \(2014\)](#) suggests using different thresholds for different forecast horizons, ranging from 0.3 to 0.44. [Vrontos et al. \(2021\)](#) adopt a fixed threshold of 0.33 for classification and evaluation purposes. In the case of neural networks, they are assumed to be capable of capturing the asymmetry and other nonlinear characteristics of business cycles. Furthermore, they need to be compared to linear frameworks to assess their predictability. Hence, for comparison purposes, I opt to follow the traditional approach and use a fixed threshold of 0.5 for all the models in this study.

The model is reestimated for the entire out-of-sample period to capture dynamic structural changes in the data. To manage computational resources, a forecast window of 12 months is selected, during which the estimated parameters remain constant. This means that once a neural network model is built, it is used to predict for the next 12 months using the latest available data. Afterward, the observed data for those 12 months is added to the existing sample, and the

neural network model is reestimated using this extended dataset. The updated parameters are then used to forecast for the following 12 months, and so on. Although this repeated estimation approach is time-consuming and costly, it mimics the real-time process of generating predictions using the most up-to-date data available. To clarify this procedure, I focus on the nowcasting forecasts. The out-of-sample period begins in November 2006, and I want to predict for that month. In November 2006 data up to September 2006 are available. The training and validation set consists of 476 monthly observations from February 1967 to September 2006. Using the optimized hyperparameters obtained through time series cross-validation, I compute the nowcasting forecast for November 2006. The same model uses the most recent data available each month to generate predictions for the next 12 months. For the next iteration, data of the last 12 months are added to the training and validation set. The model is reestimated and used to predict for November 2007 and onwards. This expanding window procedure is repeated, gradually increasing the size of the training and validation set, to generate out-of-sample forecasts for the test period spanning from November 2006 to October 2021. The same approach is adopted for the other forecast horizons.

3.3. Performance evaluation

The estimated models produce two types of forecasts, probability and point predictions. The models first generate probability predictions. In the next step, these probabilities are transformed into binary point predictions using a specified threshold. While the second type may not always be necessary, it is included to ensure the forecast is more easily interpretable for the end-users. The performance of both the probability and point predictions is evaluated using various statistical measures. With the exception of metrics specifically related to probability predictions, the evaluation is based on the output of a contingency table, commonly known as a confusion matrix as illustrated in Table 4. This matrix provides a framework for assessing the accuracy of the point predictions.

The confusion matrix is composed of elements that represent the count of observations belonging to different categories. True positives (TP) and true negatives (TN) indicate the correct classification of positive and negative outcomes, respectively. False positives (FP) occur when the prediction is positive while the actual value is negative. Conversely, false negatives (FN) arise when the prediction is negative while the actual value is positive. By utilizing these counts, various performance evaluation measures are derived to assess the overall performance of the models.

Table 4: Confusion Matrix

		Predicted	
		Positive	Negative
Actual	Positive	TP	FN
	Negative	FP	TN

The table contains elements representing the count of observations belonging to each category. True positives (TP) and true negatives (TN) indicate the correct classification of positive and negative outcomes, respectively. False positives (FP) occur when the prediction is positive, but the actual value is negative. Conversely, false negatives (FN) arise when the prediction is negative, but the actual value is positive.

Table 5: Performance evaluation metrics

Type	Metric	Formula
Probability Prediction	Area under the ROC curve	$\int_0^1 ROC(c) dc$
	Area under the PR curve	$\int_0^1 PR(c) dc$
Point Prediction	Sensitivity	$\frac{TP}{TP+FN}$
	Specificity	$\frac{TN}{FP+TN}$
	Precision	$\frac{TP}{TP+FP}$
	Balanced accuracy	$\frac{Sensitivity+Specificity}{2}$
	Matthews correlation coefficient	$\frac{TP \times TN - FP \times FN}{\sqrt{(TP+FP)(TP+FN)(TN+FP)(TN+FN)}}$
	F_1 -Score	$\frac{2}{\frac{1}{Sensitivity} + \frac{1}{Precision}}}$

The table reports the metrics used for the performance evaluation of a forecasting model. They are divided into two groups, depending on which type of predictions they refer to.

Table 5 reports the list of the metrics for the performance evaluation. A carefully selected set of statistical metrics is used to assess the performance from different perspectives. The metrics, Area Under the Receiver Operating Characteristic Curve (AUROC) and Area Under the Precision-Recall Curve (AUPRC) are employed to measure the models' raw performance in the sense that these metrics do not require any threshold to convert probabilities into binary outcomes, making them suitable for evaluating the models' pure performance. The Receiver Operating Characteristics

(ROC) curve displays the entire set of possible combinations of true positive rates $TPR(c) = \frac{TP(c)}{\# \text{ Actual Positive}}$ and false positive rates $FPR(c) = \frac{FP(c)}{\# \text{ Actual Negative}}$ for some cutpoint $c \in (0, 1)$ that maps the predicted probability to a binary category. Similarly, the Precision Recall (PR) curve plots the complete set of possible combinations of precision and recall for $c \in (0, 1)$, where recall is a synonym for sensitivity. Both the area under the ROC curve and the PR curve increase with the underlying metrics for a given cutpoint. By aggregating over the entire set of cutpoints, these curves deliver a framework to assess the pure predictive ability of a forecasting model. [Tharwat \(2021\)](#) provides a comprehensive overview of other metrics, while chapter 2 briefly discusses their strengths and weaknesses, particularly in the context of imbalanced binary classification problems.

4. Empirical results

Table 6 presents the out-of-sample forecast performance of the models for various forecast horizons. The performance values of the logit and ridge logit models, obtained from chapter 2, are included in the analysis after applying a fixed threshold of 0.5, and can now be directly compared to the neural network models in this study since they are based on the same data and forecast horizons.

In the nowcasting setup, there is a difference in predictive performance between the types of logit models and neural network models. The standard logit model is not outperforming other models in any considered metric, although the difference is smaller compared to other forecast horizons. The ridge logit model performs similarly to FFN. Although FFN performs slightly better, the differences are small for most of the metrics. However, LSTM and GRU show significantly better performance in terms of MCC and F_1 -Score, mainly due to their high precision values. For instance, LSTM correctly identifies 90% of recession months, while 75% of its positive predictions are correct. In contrast, the ridge logit model has a precision of 51.5%, indicating that LSTM accurately predicts recessions without generating too many false alarms. The AUPRC values also highlight the superiority of LSTM and GRU models over the others, with GRU achieving an AUPRC of 0.837 compared to 0.642 for FFN and 0.529 for the ridge logit model. [Davis and Goadrich \(2006\)](#) argue that PR curves give a more informative picture of an algorithm's performance, when dealing with imbalanced dataset. In fact, the ratios of the number of months in booms to the number of months in recessions in 194 real-time vintages range from 4.5 to 6.7 with a mean value of 6, which

Table 6: Performance evaluation measures: A real-time assessment

Method	AUROC	AUPRC	BAcc	MCC	F_1 -Score	Sensitivity	Specificity	Precision
Panel A: nowcasting setup								
Logit	0.853	0.365	0.812	0.496	0.546	0.750	0.874	0.429
Ridge	0.920	0.529	0.875	0.597	0.630	0.850	0.893	0.500
FFN	0.917	0.642	0.906	0.668	0.692	0.900	0.912	0.563
LSTM	0.899	0.754	0.931	0.797	0.818	0.900	0.962	0.750
GRU	0.890	0.837	0.928	0.778	0.800	0.900	0.956	0.720
Panel B: immediate-term setup								
Logit	0.671	0.243	0.634	0.230	0.327	0.400	0.868	0.276
Ridge	0.931	0.555	0.881	0.634	0.667	0.850	0.912	0.548
FFN	0.860	0.652	0.825	0.623	0.667	0.700	0.950	0.636
LSTM	0.847	0.514	0.890	0.607	0.632	0.900	0.881	0.487
GRU	0.896	0.831	0.944	0.887	0.900	0.900	0.987	0.900
Panel C: short-term setup								
Logit	0.524	0.170	0.587	0.156	0.261	0.300	0.874	0.231
Ridge	0.928	0.522	0.850	0.575	0.615	0.800	0.899	0.500
FFN	0.872	0.800	0.841	0.732	0.757	0.700	0.981	0.824
LSTM	0.858	0.395	0.784	0.508	0.565	0.650	0.918	0.500
GRU	0.885	0.544	0.931	0.797	0.818	0.900	0.962	0.750
Panel D: medium-term setup								
Logit	0.632	0.174	0.515	0.029	0.143	0.150	0.881	0.136
Ridge	0.910	0.423	0.840	0.541	0.582	0.800	0.881	0.457
FFN	0.795	0.496	0.731	0.510	0.556	0.500	0.962	0.625
LSTM	0.853	0.519	0.903	0.655	0.679	0.900	0.906	0.546
GRU	0.731	0.250	0.647	0.266	0.356	0.400	0.893	0.320
Panel E: long-term setup								
Logit	0.737	0.250	0.625	0.235	0.326	0.350	0.899	0.304
Ridge	0.818	0.388	0.668	0.265	0.357	0.500	0.837	0.278
FFN	0.856	0.365	0.612	0.235	0.316	0.300	0.925	0.333
LSTM	0.862	0.371	0.725	0.396	0.468	0.550	0.899	0.407
GRU	0.909	0.674	0.837	0.707	0.737	0.700	0.975	0.778

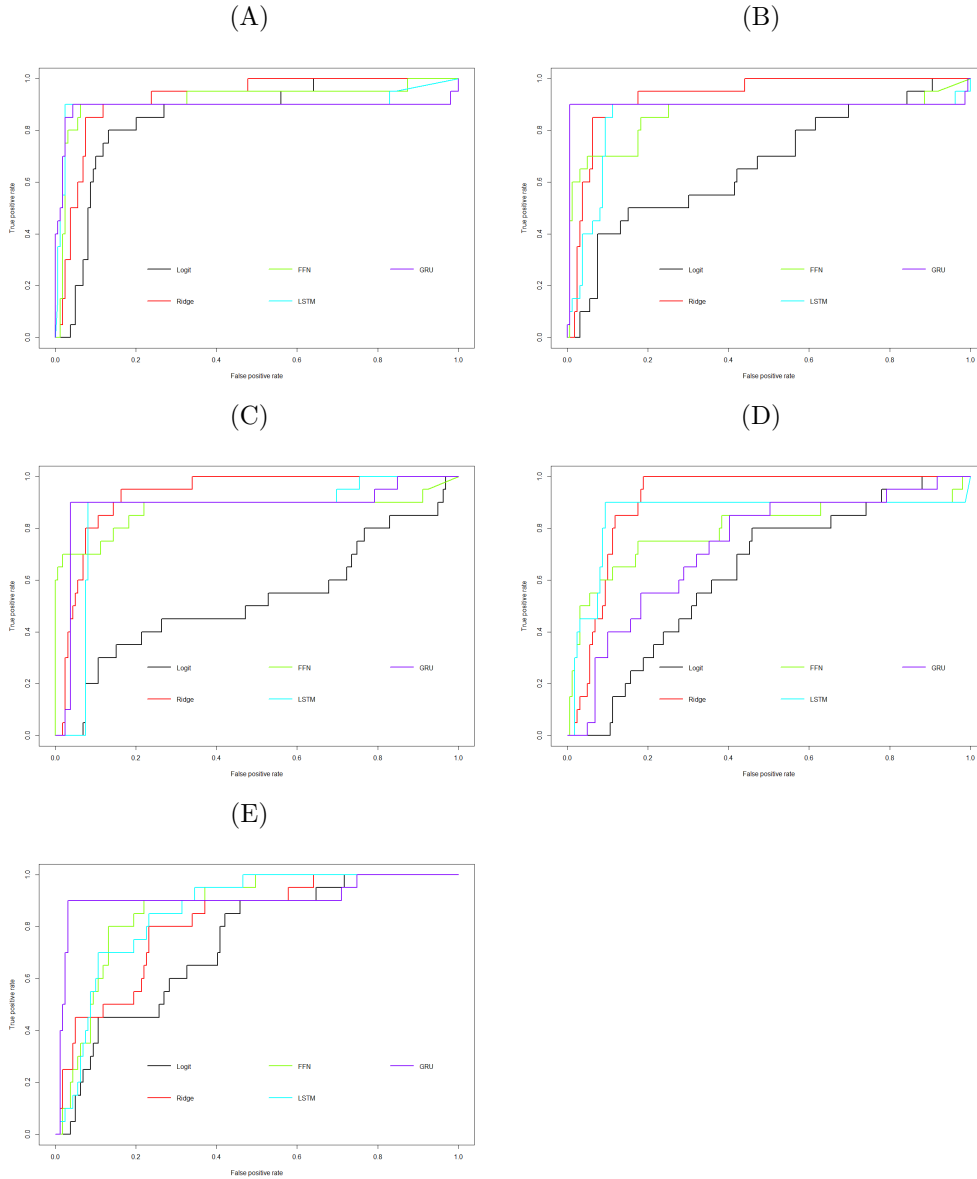
The table reports the performance evaluation measures of forecasts obtained by logit models, ridge logit models, feed-forward (FFN), long short-term memory (LSTM), and gated recurrent unit (GRU) neural networks over different forecast horizons for the out-of-sample period, November 2006 to October 2021: Panel (A) presents the nowcasts. Panel (B), (C), (D), and (E) display the 1-months-ahead forecasts, the 3-months-ahead forecasts, the 6-months-ahead forecasts, and the 12-month-ahead forecasts, respectively.

means that the period of booms is in average 6 times longer than that of recessions. The percentage of recessions in the datasets fluctuates around 0.2 across the vintages. Although not extremely skewed, the datasets are certainly imbalanced, and the difference in AUPRC values suggests that LSTM and GRU are better at extracting hidden patterns from scarce data of recessions.

Moving to the immediate-term setup, logit models perform significantly worse, with MCC and F_1 -Score approximately 40% lower than before. Conversely, the other models show similar or slightly improved performance. Among them, GRU exhibits the highest performance across various summarizing metrics such as balanced accuracy, MCC, and F_1 -Score. In the short-term setup, although the ridge logit model demonstrates better predictive performance than LSTM, on average, neural network models, particularly GRU, outperform the other models. GRU maintains a 90% accuracy in classifying recession months with higher specificity and precision, resulting in higher values of balanced accuracy, MCC, and F_1 -Score. In the medium-term setup, LSTM performs slightly better than the other models, while GRU performs poorly, and thus the difference between the two groups is minimal. However, LSTM achieves 90% sensitivity and over 90% specificity, while maintaining precision above 0.5. The overall average performance of the models is the lowest among different forecast horizons. In the long-term setup, GRU surpasses the other models by a significant margin, with an F_1 -Score of 0.737 compared to 0.468 for LSTM and 0.357 for the ridge logit model. GRU still accurately predicts 70% of recession months, with 77.8% of its positive predictions being correct.

Neural network models, especially LSTM and GRU, show a significant improvement in predictive performance compared to logit models. Across all metrics considered, neural network models consistently outperform logit models by a significant margin, except for the nowcasting setup. This superiority is evident in both pure performance metrics such as AUROC and AUPRC, as well as threshold-based point prediction metrics. The disparity is particularly prominent in AUPRC, which is a more reliable indicator when dealing with imbalanced data, highlighting the neural network models' ability to handle class imbalance effectively. The performance difference decreases when comparing them to ridge logit models. Ridge logit models exhibit higher AUROC values compared to other model specifications, except for the long-term setup. However, in terms of AUPRC, neural networks again prove to be a better choice. On average, neural network models perform better than ridge logit models in terms of these metrics. The gap widens further when considering only

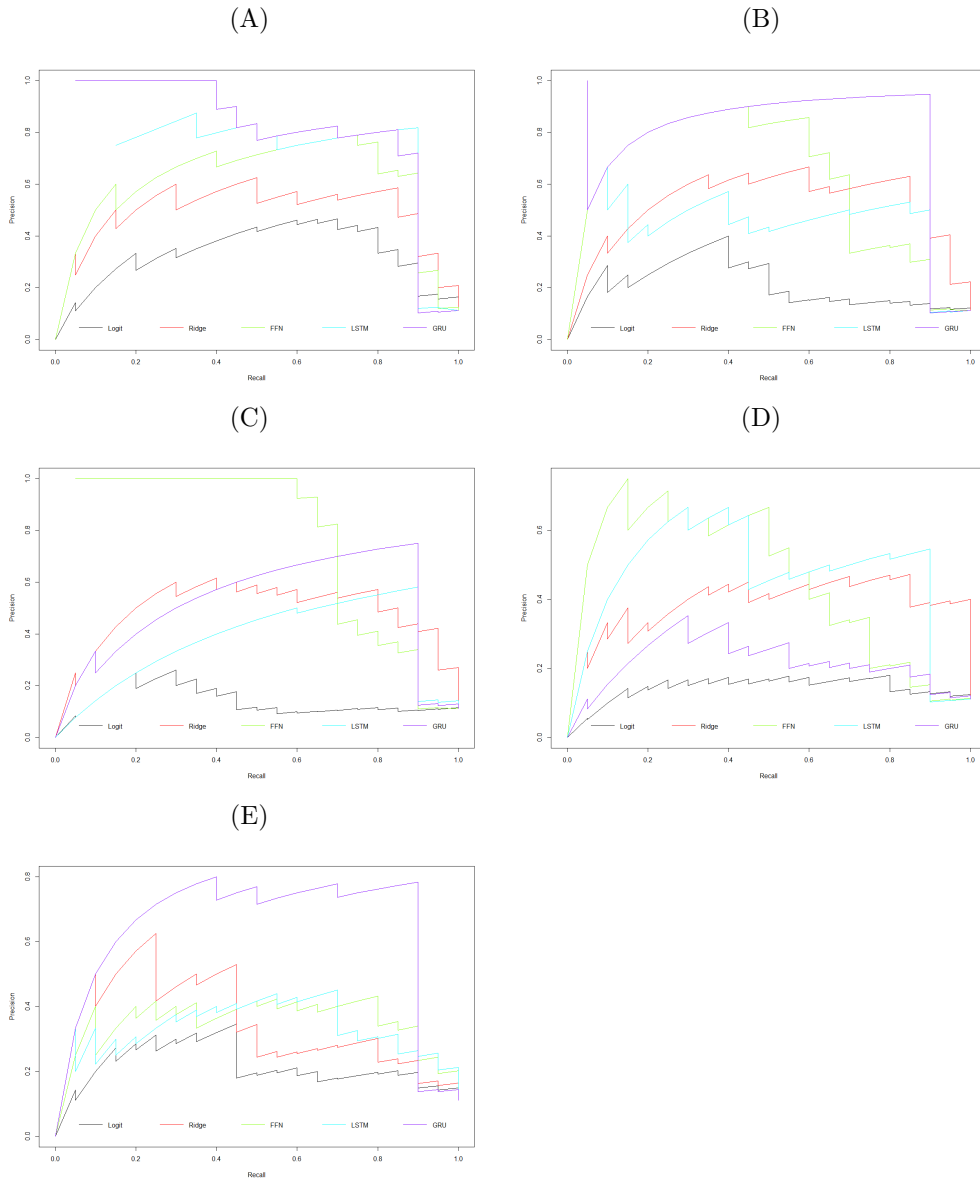
Figure 6: Receiver Operating Characteristic (ROC) curves



The figure illustrates receiver operating characteristic (ROC) curves for the out-of-sample period from November 2006 to October 2021: Panel (A) shows the ROC curves for the nowcasting forecast horizon, comparing the logit model, ridge logit model, FFN, LSTM, and GRU. Panels (B), (C), (D), and (E) present the ROC curves for the immediate-term (1-months-ahead), short-term (3-months-ahead), medium-term (6-months-ahead), and long-term (12-months-ahead) forecast horizon, respectively.

the two recurrent neural network models. Depending on the forecast horizons, either LSTM or GRU may lead the competition, with occasionally substantial differences between them and the

Figure 7: Precision Recall (PR) curves



The figure depicts precision recall (PR) curves for the out-of-sample period from November 2006 to October 2021: Panel (A) shows the PR curves for the nowcasting forecast horizon, comparing the logit model, ridge logit model, FFN, LSTM, and GRU. Panels (B), (C), (D), and (E) present the PR curves for the immediate-term (1-months-ahead), short-term (3-months-ahead), medium-term (6-months-ahead), and long-term (12-months-ahead) forecast horizon, respectively.

other models.

The ROC and PR curves of the models for five different forecast horizons are presented in

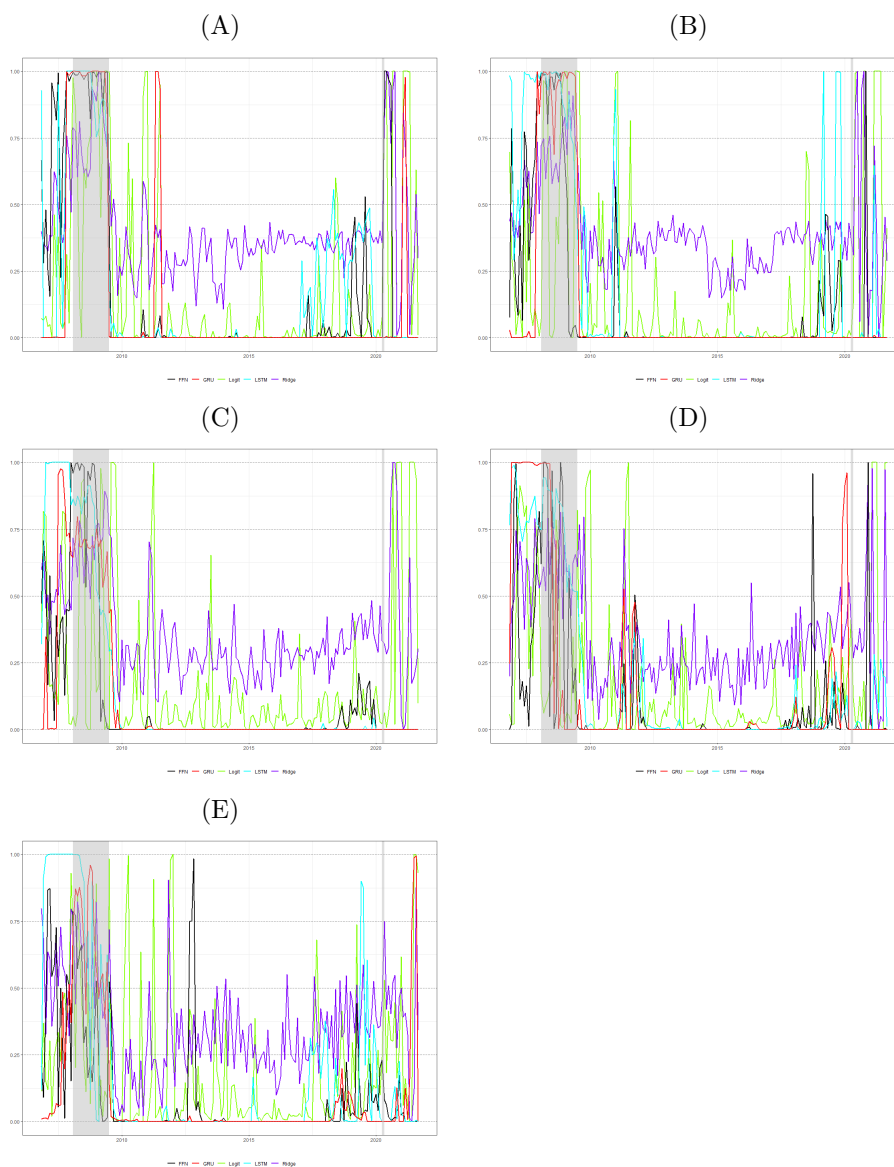
Figure 6 and 7, respectively. Panel B and C of the ROC curves highlight the noticeable difference in forecast performance between the logit model (represented by the black line) and the other models. In Panel D and E, although the lines are closer together, there is still some discernible gap between each of the models. Overall, the ridge logit model, LSTM, and GRU exhibit superior performance of probability predictions across various forecast horizons. In Figure 7 demonstrates that, the green, blue, and purple lines lie, on average, above the red line and, even more so, above the black line. This finding supports the argument that neural network models, compared to linear models, are more capable of handling class imbalance in the data.

Figure 8 displays the out-of-sample forecasts in probabilities from November 2006 to September 2021, accompanied by the grey shaded areas representing the Great Recession and the Covid-19 recession. Across all panels, similar patterns emerge: the graphs start at high levels before the Great Recession, either remain high or increase during that period, decrease afterward to a range between 0 and 0.25 for an extended period, and then exhibit significant fluctuations around the Covid-19 recession. The models successfully indicate economic and financial downturns during the Great Recession, but an external event like the Covid-19 recession remains largely unpredictable. Depending on the forecast horizon, once the model learns from the impact of the Covid-19 pandemic on the economy, it struggles to interpret this abrupt change and generates alternating forecasts.

5. Variable importance

To gain a better understanding of the underlying factors driving the results, it is important to identify the main variables that have the most significant impact on the prediction. While linear models can refer to estimated coefficients or marginal effects to measure variable importance, more complex models like neural networks require different approaches. [Molnar \(2020\)](#) provides a comprehensive list of methods that enable the interpretation of complex machine learning models. One such method is Local Interpretable Model-Agnostic Explanations (LIME), which suggests the use of other interpretable models to approximate the predictions locally. For an instance of interest, LIME constructs a new dataset by altering samples variable-wise, drawing from a normal distribution with sample mean and sample standard deviation, and obtains corresponding predictions from the black box model. This modified dataset is then used to train an interpretable model, such as Lasso or a decision tree, which is weighted by the proximity of the sampled instances

Figure 8: Out-of-sample recession probabilities



The figure presents out-of-sample recession probabilities for the period from November 2006 to October 2021:: Panel (A) displays the predicted recession probabilities for the nowcasting forecast horizon, comparing the logit model, ridge logit model, FFN, LSTM, and GRU. Panels (B), (C), (D), and (E) show the predicted recession probabilities for the immediate-term (1-months-ahead), short-term (3-months-ahead), medium-term (6-months-ahead), and long-term (12-months-ahead) forecast horizon, respectively. The grey shaded areas depict NBER recession months.

to the instance of interest. The interpretable model serves as an approximation of the black box model's predictions at a local level, even though it may not accurately represent the global

approximation.

Another solution stems from cooperative game theory, particularly the Shapley value introduced by [Shapley \(1953\)](#). The Shapley value method involves assigning payouts to players based on their contribution to the overall payout. This cooperative framework resembles a game where players form coalitions and receive profits based on their cooperation. In the context of model predictions and their interpretability, the game pertains to the prediction task, and the payout represents the difference between the actual prediction for that data point and the average prediction across all data points. The players correspond to the variable values of the data point, working together to achieve the payout, which means predicting a specific value. To calculate the Shapley value for a specific variable value, all possible coalitions of variable values, excluding the variable of interest, are formed for each data point. The variable values outside a coalition are substituted with random values of those variables from data to generate a prediction. The predictions are computed for each coalition, both with and without the variable value of interest. The difference between these predictions represents the marginal contribution of the variable value for that coalition. This computation is repeated for all possible coalitions, and the average of the marginal contributions across all coalitions yields the Shapley value for that variable value. Finally, the Shapley values for a variable can be averaged across data points to assess the relative importance of variables in comparison to each other.

The Shapley value stands out as the sole explanation method supported by a robust theory that satisfies the axioms of efficiency, symmetry, dummy, and additivity to allow for fair distribution of the contributions among the variables ([Molnar \(2020\)](#)). Conversely, methods like LIME rely on the assumption of local linear behavior of the machine learning model, but lack a theoretical justification for why this approach is effective. [Lundberg and Lee \(2017\)](#) propose an alternative estimation method, the Shapley additive explanations (SHAP), which uses a kernel-based estimation approach for Shapley values (KernelSHAP). SHAP introduces an innovative aspect by presenting the Shapley value explanation in the form of an additive variable attribution method, which can be viewed as a linear model. This perspective establishes a connection between LIME and Shapley values. In this context, SHAP defines the explanation model as follows:

$$f(c') = \alpha_0 + \sum_{j=1}^K \alpha_j c'_j$$

In the provided equation, the explanation model is denoted as f , the coalition vector as $c' \in \{0, 1\}^K$, the maximum coalition size as K , and the Shapley value for a variable j represented by α_j . The coalition vector c indicates the presence or absence of variable values, with a value of 1 representing presence and 0 indicating absence.

KernelSHAP is a method that estimates the contributions of individual variable values to the predictions by first generating a random coalition $c' \in \{0, 1\}^K$ consisting of K members by flipping a coin multiple times until we obtain a sequence of 0's and 1's. The sampled coalition of size K is then used as a data point for the regression model. In this model, the target is the prediction for a coalition, whereby in case of $c_k = 0$, the absent variable value is substituted with random variable values from the data. This process is repeated for each data point. Then Shapley compliant weights are computed according to the SHAP kernel that is proposed by [Lundberg and Lee \(2017\)](#). Finally, a weighted linear regression model is fitted on the modified data, and the estimated coefficients of the model are the Shapley values.

The main distinction from LIME lies in how instances are weighted in the regression model. In LIME, the weighting is determined based on the proximity of instances to the original instance. The closer an instance is, the higher its weight in LIME. On the other hand, SHAP assigns weights to sampled instances based on the weight they would receive in the Shapley value estimation. Small coalitions (with fewer 1's) and large coalitions (with many 1's) receive the highest weights in SHAP. The underlying intuition is that the most knowledge about individual variables can be obtained when their effects can be studied in isolation. For a coalition consisting of a single variable, the isolated main effect of that variable on the prediction can be observed. When a coalition includes all variables except one, it reports the total effect of that particular variable, including both the main effect and variable interactions. However, if a coalition comprises half the variables, it provides limited insight into the contribution of an individual variable due to the numerous possible coalitions with half of the variables.

The SHAP values for logit models are computed by the KernelSHAP method using KernelExplainer from SHAP package in python, whereas the SHAP values for deep learning models are approximated by an enhanced version of the DeepLIFT algorithm introduced by [Shrikumar et al.](#)

(2017) using DeepExplainer from the same package. DeepLIFT is a method used to analyze the output prediction of a neural network for a specific input. It achieves this by backpropagating the contributions of all units in the network to each input variable. DeepLIFT compares the activation of each unit to its reference activation, where for each variable, its sample mean is used as the reference input, and assigns contribution scores based on the difference between them. Unlike other approaches, DeepLIFT has the ability to uncover dependencies that may be overlooked. It can also consider positive and negative contributions separately. Additionally, the scores can be efficiently computed in a single backward pass.

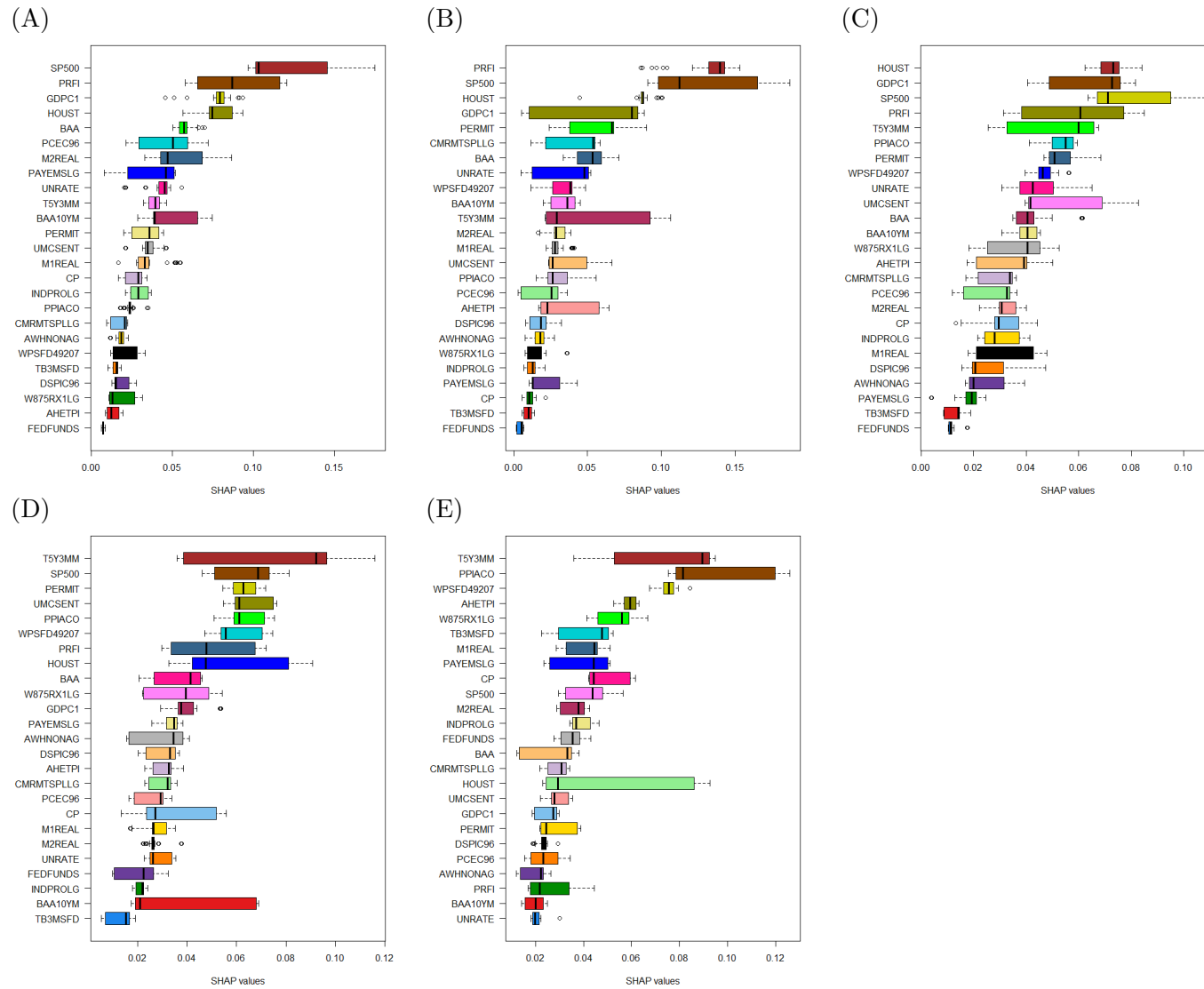
SHAP method generates a matrix of Shapley values based on the number of data points and variables. These Shapley values can be used to create global explanations by averaging the absolute Shapley values per variable across the twelve time steps and data points. This process is repeated for the entire out-of-sample period. To compare the SHAP results of neural network models to linear models, GRU and the ridge logit model are selected for the subsequent analysis, as they perform better than the others in their respective groups of models. The results for GRUs are presented in Figure 9, which depicts the distribution of average absolute SHAP values across variables. The variables are ranked based on their medians, providing insights into their importance for different forecast horizons.

The ranking of variables may vary over time, but it offers an initial understanding of the key drivers influencing the prediction results for different forecast horizon. Variables associated with financial conditions such as S&P 500 index and term spread, and macroeconomic variables related to GDP, inflation, and house market, which are commonly regarded as important recession indicators, consistently rank high (Estrella and Mishkin (1998)). These findings provide valuable insights into the black box and suggest that neural networks effectively capture the patterns inherent in the dynamics of the frequently cited recession indicators.

Figure 10 presents the SHAP results for ridge logit model. There are three major differences, among others, between the results in Figure 9 and 10. Firstly, the order of variables differs for each forecast horizon between the two types of models. While some variables appear in the leading groups for both models, their specific order varies significantly. For instance, the money supply M2 is influential in the ridge model but less prominent in the GRU model. Spearman's rank correlations between them range from -0.24 to 0.10, indicating weak correlation.

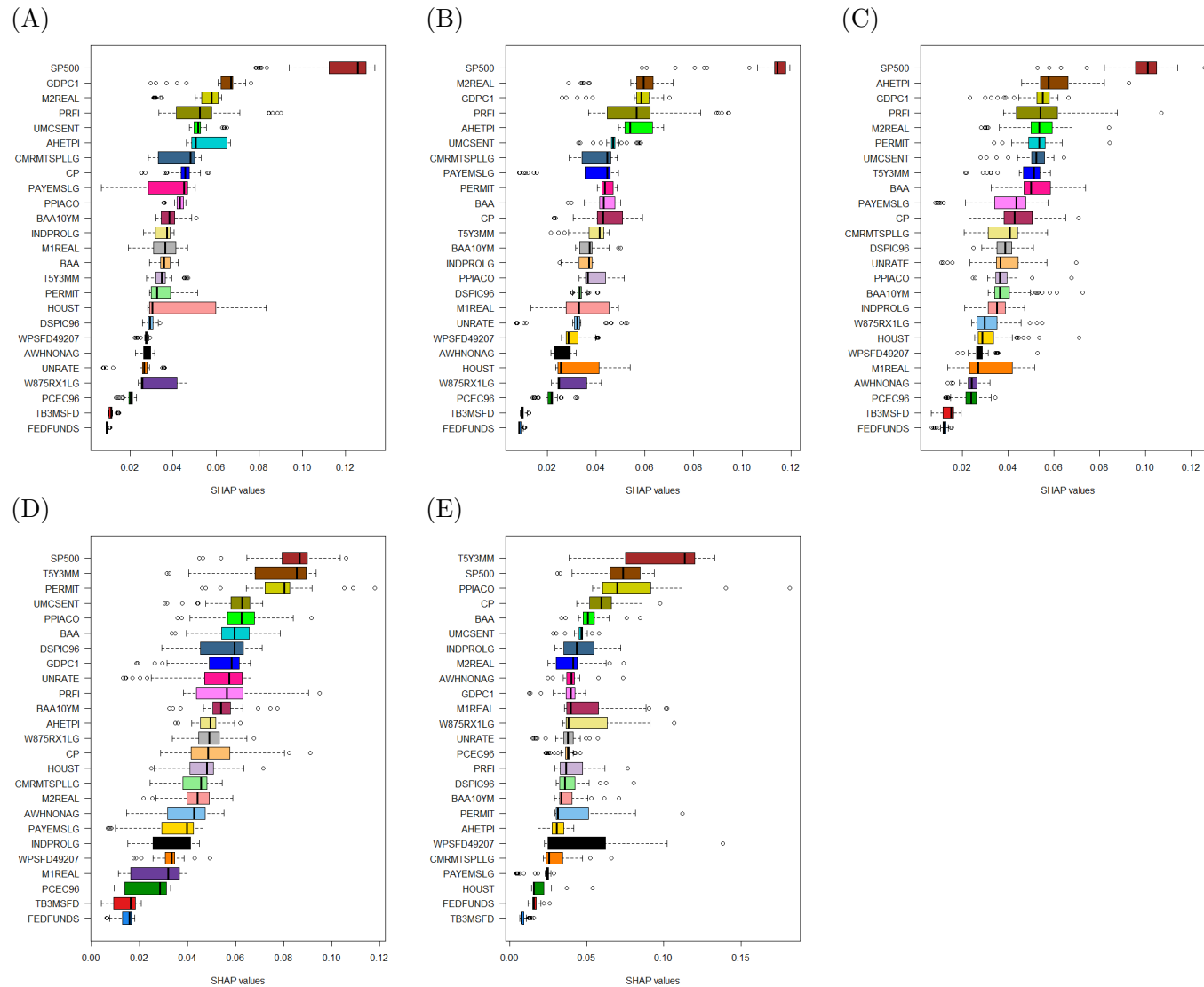
Figure 9: SHAP values of the predictors: GRU

36



The figure presents the boxplots of the GRU-based absolute average SHAP values of the predictors and their medians in descending order: Panel (A) to (E) display absolute average SHAP values of the predictors for the nowcasting, immediate-term (1-month-ahead), short-term (3-months-ahead), medium-term (6-months-ahead), and long-term (12-months-ahead) forecast horizon, respectively.

Figure 10: SHAP values of the predictors: ridge logistic regression

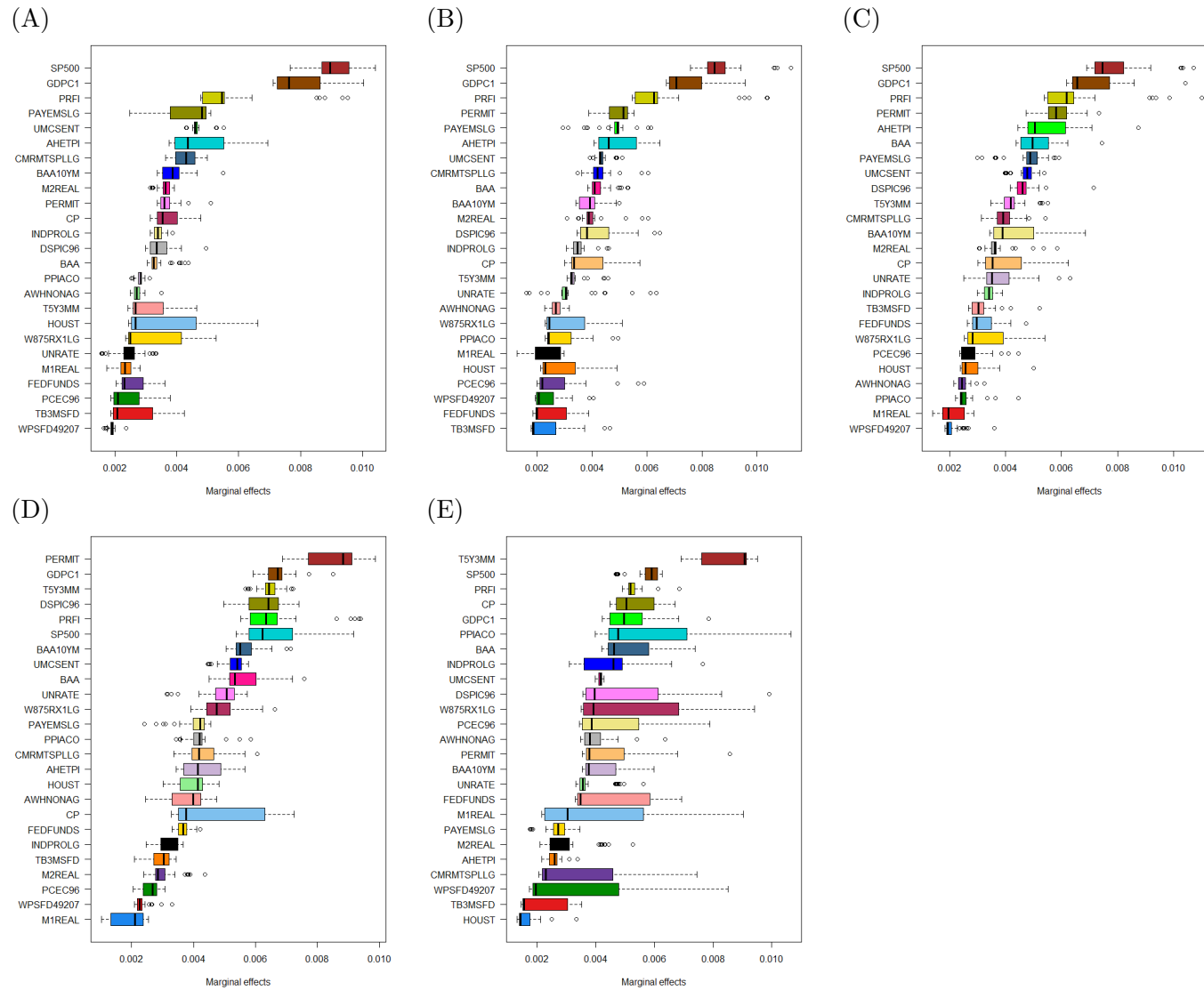


The figure shows the boxplots of the ridge model-based absolute average SHAP values of the predictors and their medians in descending order: Panel (A) to (E) display absolute average SHAP values of the predictors for the nowcasting, immediate-term (1-month-ahead), short-term (3-months-ahead), medium-term (6-months-ahead), and long-term (12-months-ahead) forecast horizon, respectively

This suggests that GRU and ridge models assign different weights to the variables. This difference could be attributed to the neural network's ability to capture nonlinear relationships, allowing for varied weighting of the variables based on different patterns. Secondly, the SHAP values of the GRU models exhibit a more even distribution among the variables compared to the ridge model. This is reflected in the smaller variation in medians between the variables. The distinction becomes particularly pronounced in the short-term setting (up to 3 months), where the ridge model heavily depends on the S&P 500 index. Additionally, the ridge model exhibits numerous outliers in the SHAP values, indicating its high sensitivity to changes in macroeconomic and financial conditions in SHAP value estimation. In contrast, this highlights GRU as a more robust modelling framework. Finally, the within variation of the GRU-based SHAP values for some variables are significantly larger than those of the others. Certain variables demonstrate little change in their SHAP values, while others exhibit significant variation. This phenomenon is less prominent in the outcomes of the ridge model. The variances are more uniformly spread, evident in the roughly equal sizes of boxes across variables. This could be viewed as another indication of the GRU's more resilient modeling framework. The GRU is capable of adapting to shifts in economic conditions, adjusting the weights of specific variables accordingly. In contrast, the ridge model has relatively fixed variable orders, with limited flexibility for variation.

The marginal effect analysis is another option to evaluate the variable importance of linear models. Since deep learning models can not be interpreted in terms of marginal effects, the average marginal effects of the ridge model are computed for the out-of-sample period and plotted in Figure 11. The Spearman's rank correlations between the variable series for the ridge model, evaluated using either SHAP values or marginal effects, range from 0.22 to 0.51. The magnitudes of the correlations are not especially large, but the previous findings, especially the first one about the leading recession indicators, also apply to the ridge model evaluated by the marginal effects. The averaged LIME values in Figure 12 which may be regarded as the marginal effect version of GRU reaffirm the main findings discussed above. The only minor distinction is that it places greater emphasis on the term spread as the comprehensive recession indicator, both in short-term and long-term contexts.

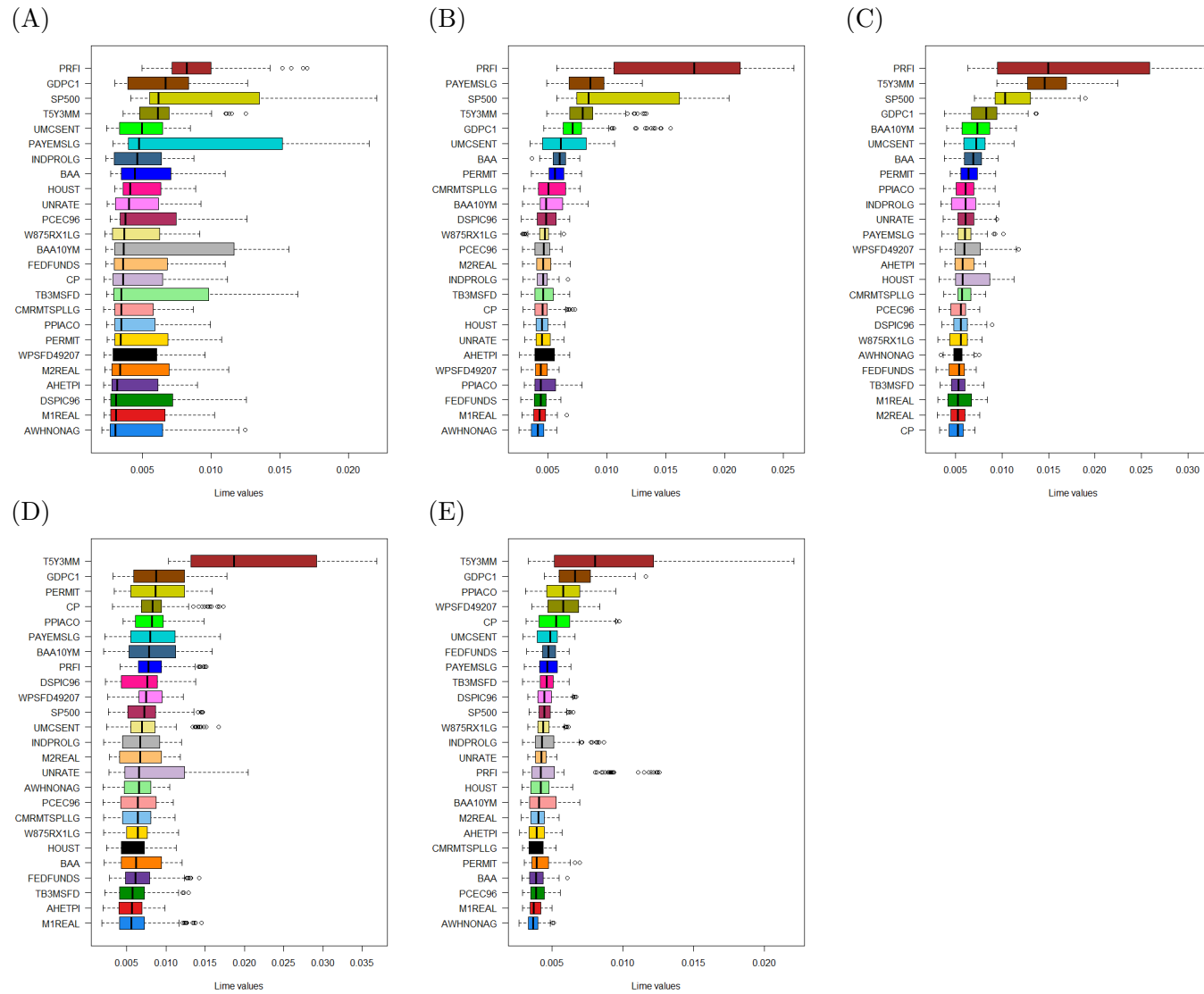
Figure 11: Marginal effects of the predictors: ridge logistic regression



39

The figure depicts the boxplots of the ridge model-based marginal effects of the predictors and their medians in descending order: Panel (A) to (E) display marginal effects of the predictors for the nowcasting, immediate-term (1-month-ahead), short-term (3-months-ahead), medium-term (6-months-ahead), and long-term (12-months-ahead) forecast horizon, respectively

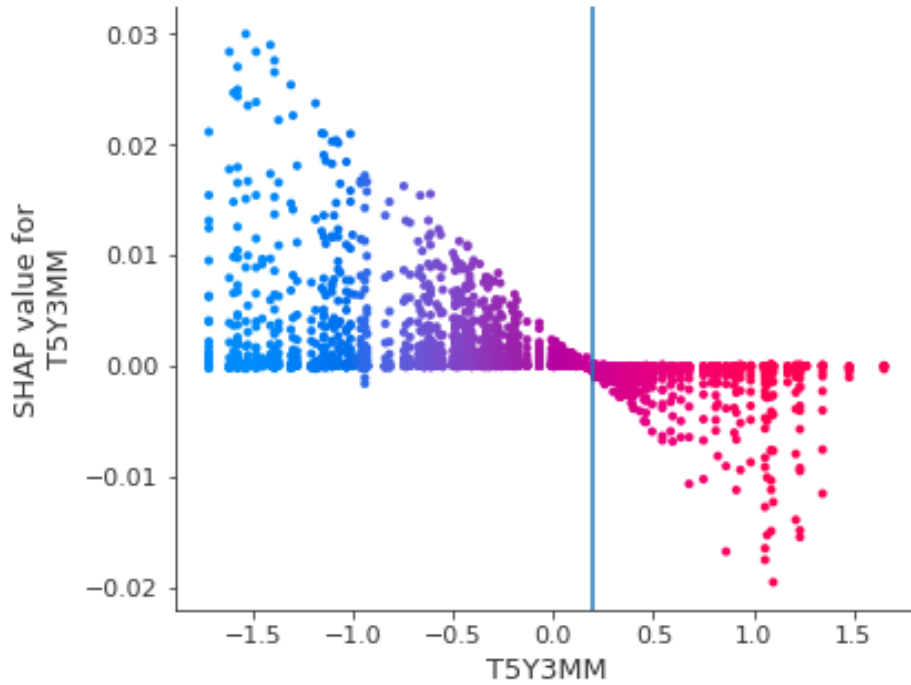
Figure 12: LIME values of the predictors: GRU



40

The figure presents the boxplots of the GRU-based absolute average LIME values of the predictors and their medians in descending order: Panel (A) to (E) display absolute average LIME values of the predictors for the nowcasting, immediate-term (1-month-ahead), short-term (3-months-ahead), medium-term (6-months-ahead), and long-term (12-months-ahead) forecast horizon, respectively.

Figure 13: Dependence plot: Term Spread



The figure plots the standardized value of the term spread on the x-axis and the corresponding SHAP value on the y-axis. The red and blue colors represent the positive and negative values of the variable, respectively.

The SHAP method allows for a detailed analysis of the impact of a single variable on predictions. In order to anticipate recessions as early as possible, I focus on the long-term forecast horizon (12 months) and consider the term spread as the most relevant and influential variable for GRU to examine its effects on recession predictions for the GRU model. Figure 13 presents the dependence plot of the term spread using the latest available data from October 2021. The x-axis represents the standardized value of the variable (term spread) while the y-axis represents the corresponding SHAP value. Notably, there is a cutoff point around 0.2, above which a higher value of the term spread has a negative impact on the predicted recession probability, while a value below the cutoff positively influences the predicted probability. Additionally, the farther the value deviates from the cutoff, the stronger the effect of the term spread on the predicted probability becomes. This corroborates the traditional interpretation of the term spread in relation to the probability of a recession according to [Estrella and Mishkin \(1996\)](#) and indicates that advanced neural network models like GRU uncovers and utilizes this relationship.

6. Conclusion

This research focuses on examining the real-time predictability of neural network models, compared to linear models, with respect to the recent two US recessions, the Great Recession and the Covid-19 recession. Three different neural network models are trained and updated throughout the study: a standard feed-forward neural network model (FFN), as well as two types of recurrent neural networks, LSTM and GRU, designed to effectively capture temporal dependencies in time series data. The performance of these models is evaluated using out-of-sample forecasts and compared to standard and ridge logit models. Additionally, the SHAP method is utilized to rank the predictors based on their importance for each forecast horizon, providing initial insights into the most influential predictors. The results are then compared to SHAP results obtained from the ridge logit model. The main findings are validated using both the LIME approach and the marginal effect method. For in-depth analysis, the most influential variable for the long-term forecast horizon, which is the term spread, is chosen to investigate the impact of the variable on the recession probability.

This paper introduces two main contributions. Firstly, it focuses on LSTM and GRU, specialized recurrent neural network models that address issues like exploding and vanishing gradients in standard recurrent neural networks. The performance of these models is compared to FFN and to the logit variants in the context of recession forecasting. Secondly, the paper employs the SHAP method to assess the variable importance in GRU and the ridge logit model for different forecast horizons. Given the commonly perceived black box nature of neural networks, the SHAP method delivers a theoretically sound framework to provide insights into the underlying rationales influencing the predictions. The three main findings are as follows: Firstly, LSTM and GRU demonstrate strong out-of-sample performance in recession forecasting across five forecast horizons, particularly excelling in long-term predictions. Secondly, there are differences in how GRU and the ridge logit model evaluate the variable importance. The variable order differs for each forecast horizon between GRU and the ridge model. While some variables are significant in both models, their specific ranking varies notably. This suggests that GRU and the ridge model assign different weights to variables, potentially due to the neural network's capacity to capture nonlinear relationships and assign varied weights based on distinct patterns. Furthermore, the SHAP values of GRU models show a more balanced distribution among variables compared to the ridge model. This is evident

in the smaller variation in medians between variables. The difference is particularly noticeable in the short-term scenario (up to 3 months), where the ridge model heavily relies on the S&P 500 index. Moreover, the ridge model displays numerous outliers in SHAP values, indicating high sensitivity to changes in macroeconomic and financial conditions. In contrast, this emphasizes GRU's robustness. The within variation of GRU-based SHAP values for some variables is significantly larger than for others. Certain variables show minimal change in SHAP values, while others exhibit considerable variation. This contrast is less pronounced in the ridge model outcomes, where variances are more evenly distributed, reflected in similar box sizes across variables. This suggests that the GRU has a more adaptable modeling framework, capable of adjusting variable weights in response to shifts in economic conditions. Conversely, the ridge model has relatively fixed variable orders, with limited flexibility for variation. Lastly, although the primary predictors for GRU and ridge logit models show slight differences, key indicators such as the S&P 500 index, real GDP, and private residential fixed investment consistently play a significant role in short-term predictions (up to 3 months). For longer-term forecasts (6 months or more), the term spread and producer price index become more prominent. These results are supported by other interpretation methods, the local interpretable model-agnostic explanations (LIME) for GRU and the marginal effects for the ridge logit model.

References

- Acemoglu, D., Scott, A., 1997. Asymmetric business cycles: Theory and time-series evidence. *Journal of Monetary Economics* 40(3), 501–533.
- Bellman, R., 1961. *Adaptive control processes: a guided tour*. Princeton University Press.
- Berge, T., Jorda, O., 2011. Evaluating the classification of economic activity into recessions and expansions. *American Economic Journal: Macroeconomics* 3(2), 246–277.
- Bergstra, J., Bengio, Y., 2012. Random search for hyper-parameter optimization. *Journal of Machine Learning Research* 13, 281–305.
- Bluwstein, K., Buckmann, M., Joseph, A., Kang, M., Kapadia, S., Simsek, O., 2020. Credit growth, the yield curve and financial crisis prediction: evidence from a machine learning approach. Working paper no. 848, Bank of England 76, 417–427.
- Bottou, L., 2010. Large-scale machine learning with stochastic gradient descent, in: *Proceedings of COMPSTAT’2010*, Springer-Verlag Berlin Heidelberg.
- Chauvet, M., Piger, J., 2008. A comparison of the real-time performance of business cycle dating methods. *Journal of Business and Economic Statistics* 26(1), 42–49.
- Chauvet, M., Potter, S., 2005. Forecasting recessions using the yield curve. *Journal of Forecasting* 24(2), 77–103.
- Cho, K., van Merriënboer, B., Gulcehre, C., Bahdanau, D., Bougares, F., Schwenk, H., Bengio, Y., 2014. Learning phrase representations using rnn encoder-decoder for statistical machine translation. In *Proceedings of the 2014 Conference on Empirical Methods in Natural Language Processing (EMNLP)* , 1724–1734.
- Davis, J., Goadrich, M., 2006. The relationship between precision-recall and roc curves. In *Proceedings of the 23rd international conference on Machine learning* , 233–240.
- De Veaux, R., Ungar, L., 1994. Multicollinearity: a tale of two nonparametric regressions. *Selecting models from data: artificial intelligence and statistics IV* , 293–302.
- Delgado, P., Congregado, E., Golpe, A., Vides, J., 2022. The yield curve as a recession leading indicator. an application for gradient boosting and random forest. arXiv: 2203.06648.
- Duchi, J., Hazan, E., Singer, Y., 2011. Adaptive subgradient methods for online learning and stochastic optimization. *Journal of Machine Learning Research* 12, 2121–2159.
- Dueker, M., 1997. Strengthening the case for the yield curve as a predictor of u.s. recessions. *Federal Reserve Bank of St. Louis Review* 79, 41–51.
- Dueker, M., 2002. Regime-dependent recession forecasts and the 2001 recession. *Federal Reserve Bank of St. Louis Review* 84(6), 29–36.
- Estrella, A., Mishkin, F., 1996. The yield curve as a predictor of u.s. recessions, current issues in economics and finance. *Federal Reserve Bank of New York Research Paper Series* 2(7), 1–6.
- Estrella, A., Mishkin, F., 1998. Predicting u.s. recessions: Financial variables as leading indicators. *The Review of Economics and Statistics* 80(1), 45–61.
- Fornari, F., Lemke, W., 2010. Predicting recession probabilities with financial variables over multiple horizons. Working paper series 1255, European Central Bank.

- Fornaro, P., 2016. Forecasting us recessions with a large set of predictors. *Journal of Forecasting* 35(6), 477–492.
- Ge, R., Huang, F., Jin, C., Yuan, Y., 2015. Escaping from saddle points - online stochastic gradient for tensor decomposition. *JMLR: Workshop and Conference Proceedings* 40, 1–46.
- Hochreiter, S., Schmidhuber, J., 1997. Long short-term memory. *Neural Computation* 9(8), 1735–1780.
- Hoerl, E., Kennard, W., 1970. Ridge regression: Applications to nonorthogonal problems. *Technometrics* 12(1), 69–82.
- Holopainen, M., Sarlin, P., 2017. Toward robust early-warning models: a horse race, ensembles and model uncertainty. *Journal of Quantitative Finance* 17(12), 1933–1963.
- Hornik, K., Stinchcombe, M., White, H., 1989. Multilayer feedforward networks are universal approximators. *Neural Networks* 2, 359–366.
- Jaditz, T., Riddick, L., Sayers, C., 1998. Multivariate nonlinear forecasting: Using financial information to forecast the real sector. *Macroeconomic Dynamics* 2, 369–382.
- Kingma, D., Ba, J., 2014. Adam: a method for stochastic optimization. arXiv: 1412.6980v9.
- Lenail, A., 2019. Nn-svg: Publication-ready neural network architecture schematics. *Journal of Open Source Software* 4(33), 747.
- Lundberg, S., Lee, S., 2017. A unified approach to interpreting model predictions. *Advances in Neural Information Processing Systems* 30.
- Maasoumi, E., Khotanzad, A., Abaye, A., 1994. Artificial neural networks for some macroeconomic series: a first report. *Econometric Reviews* 13, 105–122.
- Mitchell, W., Burns, A., 1938. Statistical indicators of cyclical revivals. *NBER Chapters: Business Cycle Indicators* (1), 162–183.
- Molnar, C., 2020. *Interpretable machine learning: A guide for making black box models explainable* 2ed. <http://christophm.github.io/interpretable-ml-book/>.
- Morley, J., Piger, J., 2012. The asymmetric business cycle. *Review of Economics and Statistics* 94(1), 208–221.
- Moshiri, S., Cameron, N., 2000. Econometric versus ann models in forecasting inflation. *Journal of Forecasting* 19(3), 201–217.
- Ng, S., 2014. Viewpoint: boosting recessions. *Canadian Journal of Economics* 47, 1–34.
- Nyberg, H., 2014. A bivariate autoregressive probit model: Business cycle linkages and transmission of recession probabilities. *Macroeconomic Dynamics* 18(4), 838–862.
- Puglia, M., Tucker, A., 2021. Neural networks, the treasury yield curve, and recession forecasting. *The Journal of Financial Data Science* 3(2), 149–175.
- Qi, M., 2001. Predicting us recessions with leading indicators via neural network models. *International Journal of Forecasting* 17, 383–401.
- Shapley, L., 1953. A value for n-person games. *Contributions to the Theory of Games II* AM-28, 307–317.
- Shrikumar, A., Greenside, P., Kundaje, A., 2017. Learning important features through propagating activation differences. *International conference on machine learning* PMLR, 3145–3153.
- Srivastava, N., Hinton, G., Krizhevsky, A., Sutskever, I., Salakhutdinov, R., 2014. Dropout: a simple way to prevent neural networks from overfitting. *Journal of Machine Learning Research* 15, 1929–1958.

- Stark, T., Croushore, D., 2002. Forecasting with a real-time data set for macroeconomists. *Journal of Macroeconomics* 24(4), 507–531.
- Stekhoven, D., Bühlmann, P., 2011. Missforest: Non-parametric missing value imputation for mixed-type data. *Bioinformatics* 28(1), 112–118.
- Stock, J., Watson, M., 1998. A comparison of linear and nonlinear univariate models for forecasting macroeconomic time series. NBER Working paper no. 6607.
- Swanson, N., White, H., 1997. A model selection approach to real-time macroeconomic forecasting using linear models and artificial neural networks. *The Review of Economics and Statistics* 79, 540–550.
- Tharwat, A., 2021. Classification assessment methods. *Applied Computing and Informatics* 17(1), 168–192.
- Tiao, G., Tsay, R., 1994. Some advances in non-linear and adaptive modelling in time-series. *Journal of Forecasting* 13, 109–131.
- Tibshirani, R., 1996. Regression shrinkage and selection via the lasso. *Journal of the Royal Statistical Society Series B*, 267–288.
- Tieleman, T., Hinton, G., 2012. Rmsprop: divide the gradient by a running average of its recent magnitude. *Neural Networks for Machine Learning* 4, 26–31.
- Tkacz, G., 2001. Neural network forecasting of canadian gdp growth. *International Journal of Forecasting* 17, 57–69.
- Vishwanathan, S., Murty, M., 2002. Ssvm: a simple svm algorithm. *Proceedings of the 2002 International Joint Conference on Neural Networks* 3 IEEE, 2393–2398.
- Vrontos, S., Galakis, J., Vrontos, I., 2021. Modeling and predicting u.s. recessions using machine learning techniques. *International Journal of Forecasting* 37, 647–671.
- Wang, Z., Li, K., Xia, S., Liu, H., 2022. Economic recession prediction using deep neural network. *The Journal of Financial Data* 4(3), 108–127.
- Wright, J., 2006. The yield curve and predicting recessions. FEDs Working Paper No. 2006-07.
- Ying, X., 2019. An overview of overfitting and its solutions. *Journal of Physics: Conference Series* 1168, 022022.
- Zhang, G., Patuwo, B., Hu, M., 1998. Forecasting with artificial neural networks: the state of the art. *International Journal of Forecasting* 14, 35–62.
- Zhang, Y., Wang, Y., Luo, G., 2020. A new optimization algorithm for non-stationary time series prediction based on recurrent neural networks. *Future Generation Computer Systems* 102, 738–745.